Nanoscale

Synthesis and Photophysical Properties of New Catenated Electron Donor-Acceptor Materials with Magnesium and Free Base Porphyrins as Donors and C60 as the Acceptor

Journal:	*Nanoscale*
Manuscript ID:	NR-ART-10-2014-006146
Article Type:	Paper
Date Submitted by the Author:	17-Oct-2014
Complete List of Authors:	Kirner, Sabrina; Friedrich-Alexander-Universitat Erlangen-Nurnberg, Department of Chemistry Guldi, Dirk; Friedrich-Alexander-Universitat Erlangen-Nurnberg, Chemistry and Pharmacy Megiatto Jr., Jackson; Arizona State University, Chemistry & Biochemistry Schuster, David; New York University, Department of Chemistry

Journal Name

RSCPublishing

ARTICLE

Synthesis and Photophysical Properties of New Catenated Electron Donor-Acceptor Materials with Magnesium and Free Base Porphyrins as Donors and C_{60} as the Acceptor

Cite this: DOI: 10.1039/xoxxoooooox

Received ooth January 2012,
Accepted ooth January 2012

DOI: 10.1039/xoxxoooooox

www.rsc.org/

Sabrina V. Kirner,[a] Dirk M. Guldi,[a] Jackson D. Megiatto, Jr.[b, c] and David I. Schuster[b]

A new series of nanoscale electron donor-acceptor systems with [2]catenane architectures has been synthesized, incorporating magnesium porphyrin (MgP) or free base porphyrin (H_2P) as electron donor and C_{60} as electron acceptor, surrounding a central tetrahedral Cu(I)-1,10-phenanthroline (phen) complex. Model catenated compounds incorporating only one or none of these photoactive moieties were also prepared. The synthesis involved the use of Sauvage's metal template protocol in combination with the 1,3–dipolar cycloaddition of azides and alkynes ("click chemistry"), as in other recent reports from our laboratories. Ground state electron interactions between the individual constituents was probed using electrochemistry and UV–vis absorption spectroscopy, while events occurring following photoexcitation in tetrahydrofuran (under both aerobic and anaerobic conditions) at various wavelengths were followed by means of time-resolved transient absorption and emission spectroscopies on the femtosecond and nanosecond time scales, respectively, complemented by measurements of quantum yields for generation of singlet oxygen. From similar studies with model catenates containing one or neither of the chromophores, the events following photoexcitation could be elucidated. The results were compared with those previously reported for analogous catenates based on zinc porphyrin (ZnP). It was determined that a series of energy transfer (EnT) and electron transfer (ET) processes take place in the present catenates, ultimately generating long-distance charge separated (CS) states involving oxidized porphyrin and reduced C_{60} moieties, with lifetimes ranging from 400 to 1060 nanoseconds. Shorter lived short-distance CS states possessing oxidized copper complexes and reduced C_{60}, with lifetimes ranging from 15 to 60 ns, were formed en route to the long-distance CS states. The dynamics of the ET processes were analyzed in terms of their thermodynamic driving forces. It was clear that intramolecular back ET was occurring in the inverted region of the Marcus parabola correlating rates and driving forces for electron transfer processes. In addition, evidence for triplet excited states as a product of either incomplete ET or back ET was found. The differences in behavior of the three catenates upon photoexcitation are analyzed in terms of the energy levels of the various intermediate states and the driving forces for EnT and ET processes.

Introduction

In natural photosynthesis the energy of sunlight is converted into chemical energy by a cascade of short-range energy (EnT) and electron transfer (ET) processes. Crucial for efficient EnT and ET is the spatial arrangement of the various light harvesting antennae and the photosynthetic reaction center.[1-6] To mimic the complex photosynthetic process, simpler model artificial photosynthetic systems have been investigated.[7] One approach that provides a suitable arrangement of the chromophores is the use of mechanically interlocked rotaxanes and catenanes with attached electron donors and electron acceptors.[8-12] Sauvage's Cu(I) template synthesis[13-17] assures a rigid structure of the catenates, due to a Cu-1,10-phenanthroline (phen) ($[Cu(phen)_2]^+$) core, in which two rings become linked as a result of tetrahedral complexation of two phens to Cu(I). Thus, a fixed distance between electron donor and electron acceptor is achieved, yielding relatively long lived charge separated states (CSS) upon irradiation.[18,19] In spite of the central $[Cu(phen)_2]^+$ core, corresponding rotaxanes remain conformationally flexible due to the unclosed ring. Flamigni et. al.[18,19] investigated the electron transfer properties of catenanes and rotaxanes with attached porphyrins, which are known for their excellent light

harvesting and electrochemical characteristics. In their studies, zinc porphyrin (ZnP) served as the electron donor, while Au(III) porphyrin (AuP^+) functioned as the electron acceptor. Schuster, Guldi and coworkers replaced AuP^+ with C_{60} as the electron acceptor in catenane and rotaxane architectures, while ZnP was retained as the electron donor.[20-26] The main advantage of C_{60} compared to AuP^+ is the much longer CSS lifetime in the corresponding ZnP/C_{60} conjugates.[20-26] Firstly, the internal reorganization energy λ of C_{60} in electron transfer reactions is very small, due to the rigid structure of C_{60}.[27] Secondly, poor solvation of C_{60} in both polar and nonpolar solvents results in very small values of the external reorganization energy even in the presence of strong electronic interactions in the ground state leading, for example, to exciplex formation.[28,29] Marcus theory[30,31] predicts that small values of λ will shift the back ET into the so-called Marcus inverted region, where higher values of the exergonic free energy for back ET are accompanied by slower rates for the process, as is the case in natural photosynthesis.[2,32-34] It is well established that long lived CSS are observed for a large variety of materials, in which C_{60} is the electron acceptor in electron donor-acceptor systems, in which porphyrins, phthalocyanines and other electron donors are linked either covalently[35] or mechanically[20-26] to the fullerene.

The present work ties in with our previous study of the zinc porphyrin-[Cu(phen)$_2$]-C_{60} catenate – see structure **10** in Scheme 1.[23] The aim was to vary the redox potentials and, in turn, the driving force for ET as well as EnT by using magnesium porphyrins (MgP) and free base porphyrins, (H_2P) respectively, in place of zinc porphyrins (ZnP). Most importantly, MgPs are much easier to oxidize than the corresponding ZnPs by over 250 mV, increasing the driving force for ET reactions to acceptors such as C_{60} in various types of electron donor-acceptor systems.[36] There have been only limited reports on electron donor-acceptor systems incorporating MgP as the electron donor and C_{60} as the electron acceptor. D'Souza and coworkers [37-40] reported that MgPs exhibit higher fluorescence quantum yields and longer excited state lifetimes than the corresponding ZnPs. From time-resolved emission studies, they found that rates of intramolecular photoinduced electron transfer from the singlet excited states of MgP-C_{60} conjugates were extremely fast, on the order of 10^{10} s^{-1}, and that the quantum yields for electron transfer to generate stabilized CSSs were close to unity. As with the corresponding ZnP conjugates, back ET rates were much slower than for initial photoinduced ET, by 2-3 orders of magnitude,[12] reflecting back ET taking place in the inverted Marcus region. MgP is closely related to the light harvesting chlorophylls in natural photosynthetic systems.[1-6] It was therefore of considerable interest to investigate the photophysics of catenated structures incorporating MgP as electron donor in place of ZnP. As a further structural variant, we also determined the properties of catenated structures, in which H_2P acts as the electron donor.

These new porphyrin–[Cu(phen)$_2$]–C_{60} catenates were synthesized in the same way as their ZnP analogs,[41] that is by a combination of 1,3-dipolar cycloaddition of azides and alkynes (CuAAC or "click" reaction) [42-44] and Sauvage's Cu(I) template synthesis.[13-17] The new electron donor-acceptor systems were thoroughly characterized with respect to their spectroscopic, electrochemical, and photophysical properties. Furthermore, model [2]-catenates lacking either porphyrins, C_{60} or both served as reference systems. Finally, the three porphyrin–[Cu(phen)$_2$]–C_{60} catenates were compared regarding their charge transfer properties upon photoexcitation, namely their CSS lifetimes and the change in efficiency of ET due to the differences in redox potentials and thermodynamic driving forces.

Results and Discussion

1. Synthesis

The catenates reported in this work were prepared following our previously reported synthetic strategy based on the combination of Sauvage's Cu(I) template approach[13-16] and the Cu(I)-catalyzed–1,3-dipolar cycloaddition of azides and alkynes (CuAAC or "click" reaction) – see Scheme 1.[42-44] Briefly, C_{60}-macrocycle **1** was dissolved in dichloromethane and a solution of [Cu(CH_3CN)$_4$][PF_6] in acetonitrile was added to it. The reaction mixture was stirred at room temperature for 30 minutes under a nitrogen atmosphere. Phen thread **2** was added as a solid to the mixture and the resulting solution was stirred for 3 hours to quantitatively yield pseudorotaxane **4**. The unsubstituted pseudo-rotaxane **5** was synthesized from appropriate precursors in a similar fashion.

The biggest challenge in the synthesis of the present catenates was the macrocyclization reaction. Although the "click reaction" has proven to be an excellent protocol to prepare many catenanes and [Cu(phen)$_2$]$^+$–based catenates, in our case Cu(I) ions might become a synthetic problem as the appended free base porphyrin could potentially coordinate with the catalytic Cu ions. Upon removal of the catalytic Cu ions from the reaction medium, the "double click" macrocyclization reaction would probably not occur. Furthermore, coordination of Cu ions to the appended group on the porphyrin would lead to copper contamination of the samples, complicating spectroscopic characterization and the photophysical investigation of our catenates. Thus, the synthesis of catenate **12**, which bears H_2P, was a major challenge using "click" chemistry. For catenates **10**, **11**, and **14**, deleterious transmetallation reactions might lead to copper contamination of the catenates as well. To circumvent these synthetic challenges, we used our special "click brew" catalyst, which contains sulfonated bathophenanthroline (**SBP**) as an auxiliary ligand.[45,46] **SBP** has two beneficial effects: On one hand, it is known to enhance the "click" reaction kinetics by stabilizing the Cu(I) catalytic species, which is crucial for the high-yield synthesis of catenates under kinetic control, as in the present case. On the other hand, **SBP** also sequesters adventitious Cu(I) ions from the reaction medium, thus preventing copper contamination of the porphyrin catenates. Indeed, the target catenates **10**, **11**, **12**, and **14** were successfully prepared and isolated following the usual workup protocols and chromatographic purification. The less problematic catenates **13** and **15**, which do not contain porphyrins were prepared using the same strategy.

^{1}H NMR analysis confirmed the structures of the new catenates. The ^{1}H NMR spectrum of **11** is virtually identical to that reported previously[23] for catenate **10**, suggesting that substitution of Mg(II) for Zn(II) in the porphyrin core does not

Journal Name RSCPublishing

ARTICLE

Scheme 1 Synthetic strategy used to afford catenates* and model compounds for the photophysical investigations.

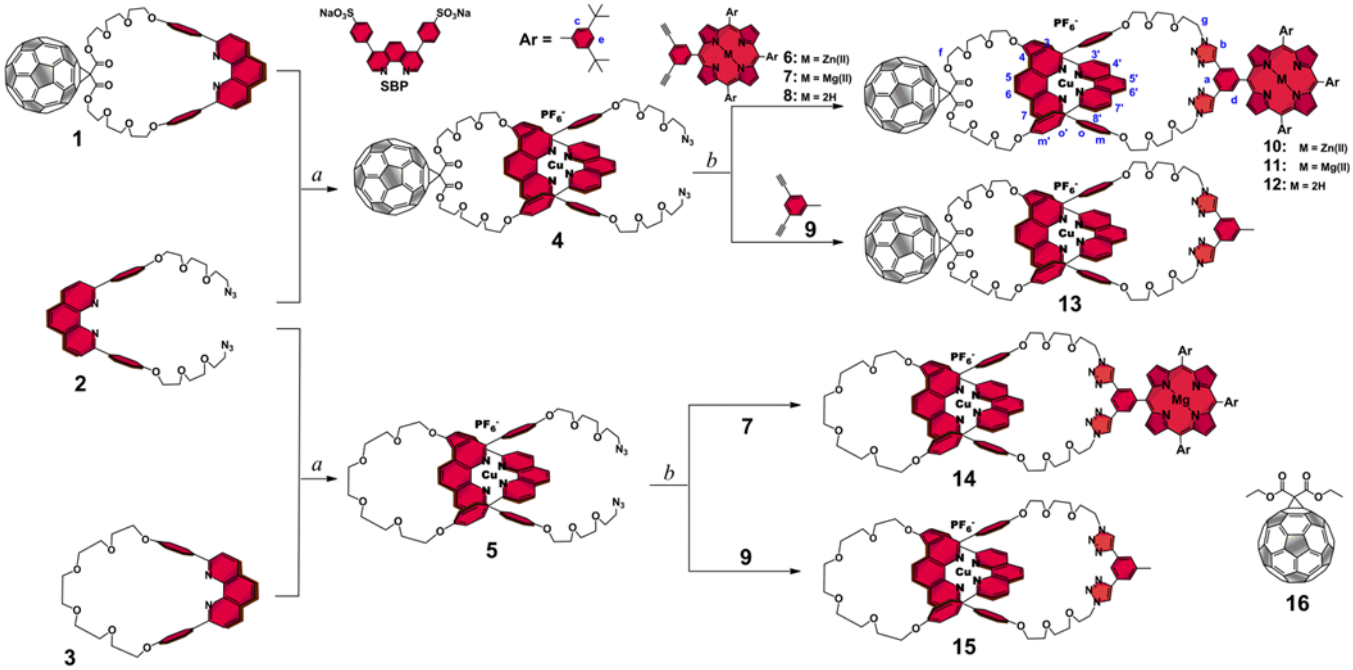

* Numbering and lettering in blue on the structures are labels for ^{1}H NMR attributions in the experimental section. Conditions for the syntheses: *(a)* $[Cu(CH_3CN)_4][PF_6]$, CH_2Cl_2/CH_3CN, rt, 3 h, quantitative; *(b)* CuI, sodium ascorbate, sulfonated bathophenathroline (SBP), DBU, H_2O/EtOH, rt, 12 h, 55-75% yields.

cause conformational changes in the catenate structure. The presence of sharp peaks in the ^{1}H NMR spectrum of **11** confirmed that our "click brew" precluded the transmetallation reaction during the "double click" macrocyclization reaction, as the residual paramagnetic Cu(II) in the porphyrin core would cause peak broadening in the ^{1}H NMR spectra. The same is true for model catenate **14**. In the case of catenate **12**, the ^{1}H NMR spectrum presented the same sharp peaks as those observed for catenates **10** and **11**, with an extra resonance at – 2.54 ppm which is attributed to the inner protons of the free-base porphyrin moiety.[47] Furthermore, the absorption spectrum of free base catenate **12** (Fig. 1) clearly shows absorption maxima at 420 nm for the Soret and at 515, 550, 594 and 649 nm for the four Q-bands, which are typical values for free base porphyrins.[7] MALDI-TOF analysis provided further support for the structure assignment to catenates **11**, **12** and **14**. The characteristic general pattern of [2]catenates in mass spectrometry features the molecular ion as well as ion peaks corresponding to the two ring components due to fragmentation of the interlocked structure during the ionization process; this pattern was indeed observed in the MALDI-TOF spectra of catenates **11**, **12**, and **14**. These findings demonstrate that our "click brew" is a suitable medium to catalyze CuAAC reactions, while simultaneously preventing copper contamination of the porphyrin moieties.

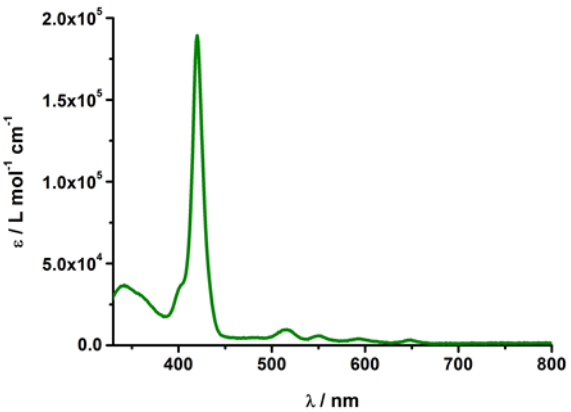

Fig.1 Absorption spectrum of catenate **12** in THF at room temperature.

2. Ground State Interactions

2.1 Electrochemistry. In order to investigate the redox properties of catenates **11** and **12** as well as the model compounds, square wave voltammetry and differential pulse voltammetry experiments were carried out in dichloromethane (DCM) as solvent in the presence of 0.1 M

Journal Name RSCPublishing

ARTICLE

Table 1 Oxidation and reduction potentials of all compounds studied. All values (V) are relative to Fc/Fc+ as internal reference. Electrolyte: 0.1 M TBAFPF6 in dichloromethane (DCM) or ortho-dichlorobenzene (o-DCB). P = porphyrin.

Compound	Solvent	Oxidation			Reduction		
		$P^{\bullet+}/P^{2+}$	$P/P^{\bullet+}$	Cu^{+}/Cu^{2+}	$C_{60}/C_{60}^{\bullet-}$	$C_{60}^{\bullet-}/C_{60}^{2-}$	C_{60}^{2-}/C_{60}^{3-}
6	*o*-DCB	0.62	0.28	–	–	–	–
7[37]	*o*-DCB	0.46	0.07	–	–	–	–
8[50]	*o*-DCB	0.79	0.53	–	–	–	–
10[23]	*o*-DCB	–	0.18	0.18	−1.12	−1.48	−1.96
11	*o*-DCB	–	−0.05	0.23	−1.19	−1.42	–
12	DCM	–	0.38	0.25	−1.07	−1.46	–
13[23]	*o*-DCB	–	–	0.16	−1.12	−1.48	−1.96
15[22]	*o*-DCB	–	–	0.16	–	–	–
16	DCM	–	–	–	−1.06	−1.44	−1.88

tetrabutylammonium hexafluorophosphate ($TBAFPF_6$) as supporting electrolyte and ferrocene/ferrocenium as internal reference. Table 1 summarizes the electrochemical data.

While the C_{60} malonate reference **16** was inactive under oxidative conditions, three one electron steps were observed under reductive conditions at –1.06, –1.44, and –1.88 V, resembling the trend found for pristine C_{60}.[48,49] Due to the partial loss of π-conjugation in **16**, a shift towards more negative values for the reduction processes is observed when compared to those of pristine C_{60}. As is known from the literature, MgP exhibits two one electron oxidation steps at +0.07 and +0.46 V.[37] H_2P, in contrast, is harder to oxidize, with oxidation potentials of +0.53 and +0.79 V.[50] Model catenate **15** reveals a single oxidation process at +0.16 V, which correlates to the one-electron oxidation of the copper center, namely $[Cu(phen)_2]^{+}/[Cu(phen)_2]^{2+}$.[18,23] C_{60}-$[Cu(phen)_2]^{+}$ catenate model **13** shows three one electron reductions in the cathodic range at –1.12, –1.48, and –1.96 V, corresponding to C_{60}. In the anodic range, the oxidation of $[Cu(phen)_2]^{+}$ is observed at +0.16 V. Thus, the presence of C_{60} has no notable impact on the $[Cu(phen)_2]^{+}$ oxidation. Overall, catenate **11** exhibits similar behavior as catenate model **13** and MgP reference **7**. In particular, two one electron reductions are detected within the electrochemical window of the solvent at –1.19 and –1.42 V. Both are assigned to C_{60}. The anodic scan reveals an oxidation at +0.23 V, which corresponds to a $[Cu(phen)_2]^{+}$ centered process, and an additional peak at –0.05 V vs. Fc/Fc^{+}. The latter stems from the first MgP oxidation. Finally, catenate **12** gives rise to the same features as those summarized for catenate **11**. In the cathodic scan, two C_{60} reductions are detected at –1.07 and –1.46 V. The anodic process reveals the $[Cu(phen)_2]^{+}$ oxidation at +0.25 V and the first H_2P oxidation at +0.38 V. In both, MgP as well as H_2P catenates **11** and **12**, the oxidation potentials of the porphyrin are shifted to lower potentials compared to the corresponding porphyrin references **7** and **8**, while the $[Cu(phen)_2]^{+}$ peaks are clearly shifted towards more positive values compared to reference **15**. The C_{60} reductions remain nearly the same in both **11** and **12** when compared to C_{60} malonate reference **16**.

2.2 UV–Vis absorption. The absorption spectra of the investigated systems show the typical features of the individual components. In Fig. 2, the spectra of MgP–catenates **11**, and **14** as well as reference **7** are dominated by the porphyrin's Soret band at 430 nm and Q-bands, which maximize between 550 and 650 nm, respectively. The absorption between 300 and 400 nm corresponds to $[Cu(phen)_2]^{+}$ in **11** and **14** and C_{60} in **11**. Importantly, the extinction coefficients, which are comparable to those seen for the references, suggest the lack of significant intramolecular electronic interactions in the ground state. A similar conclusion is gathered for H_2P–catenate **12** – see Fig. 1. Nevertheless, the main difference in **14** compared to catenate **11** is the presence of four rather than just two Q-bands in the region between 500 and 660 nm due to the different symmetry in H_2P. Furthermore, the Soret band is shifted to lower wavelengths, namely to 420 nm.

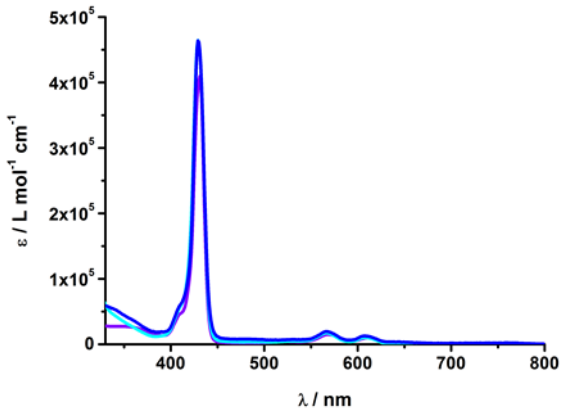

Fig.2 Absorption spectra of catenates **11** (blue), **14** (cyan) and MgP reference **7** (violet) in THF at room temperature.

3. Excited State Interactions

To investigate the electronic interactions between the different photoactive components in the excited state, steady state as well as time resolved emission and transient absorption on the femto- and nanosecond time scales were performed with catenates **11-15** and porphyrins **7** and **8** in solvents of different polarity, namely tetrahydrofuran (THF) and benzonitrile (PhCN). The data from room temperature measurements are summarized in Table 2.

3.1. Emission spectroscopy. The strongest fluorophores among the references are the porphyrins with fluorescence quantum yields (F) of 0.13 (MgP) and 0.10 (H_2P). MgP reference **7** shows emission maxima at 620 and 670 nm in THF while H_2P reference **8** exhibits red-shifted emission with maxima at 650 and 720 nm (see Fig. 3). In time resolved emission experiments, lifetimes of 11.2 and 10 ns were determined for **7** and **8**, respectively, in benzene, as shown in Table 2. $[Cu(phen)_2]^+$ reference **15** reveals much weaker emission. In PhCN, the MLCT emission has a lifetime of 2.5 ns and a quantum yield of 4.8×10^{-3} at 765 nm – Table 2 and Fig. 3. The weakest emission was observed for C_{60}–malonate **16** with a maximum at 715 nm, a fluorescence quantum yield of 1.0×10^{-3}, and a fluorescence lifetime of 1.48 ns in $CHCl_3$.[51]

Compared to the porphyrin references **7** and **8**, catenates **11**, **12**, and **14** show quenched emission. Fig. 3 depicts the emission of catenates **11** and **14** in THF solutions with equal absorptions at the 430 nm excitation wavelength. Importantly, two emission maxima at 620 and 680 nm are seen. Emissions in these catenates are quenched by approximately a factor of 2 in comparison to reference **7** – Table 2. The emission of catenate **12** is 30 nm red-shifted, which is a characteristic of free base porphyrins,[7] and is also quenched. The

Table 2 Fluorescence parameters at room temperature (293 K).

	Excited State	λ_{max} (nm)		τ_F(ns)		Φ_F		E_{00} (eV)[a]	
		THF	PhCN	THF	PhCN	THF	PhCN	THF	PhCN
6	^{1}*ZnP[b]	600	–	2.3	–	$4x10^{-2}$	–	2.09	–
7	^{1}*MgP	619	613	11.2	10.5	0.13[c]	–	2.00	2.02
8	^{1}*H_2P	650	650	10.0	11.0	0.10[c 52]	–	1.91	1.91
10	^{1}*ZnP–$[Cu(phen)_2]^+$–C_{60}[b]	603	–	0.5	–	$1x10^{-2}$	–	2.09	–
	ZnP–*$[Cu(phen)_2]^+$–C_{60}[b]	762	–	–	–	$8.6x10^{-5}$	–	1.62	–
11	^{1}*MgP–$[Cu(phen)_2]^+$–C_{60}	618	613	5.2	6.1	0.04	0.07	2.01	2.02
	MgP–*$[Cu(phen)_2]^+$–C_{60}	–	777	–	–	$5.5x10^{-4}$	$8.1x10^{-4}$	–	1.60
12	^{1}*H_2P–$[Cu(phen)_2]^+$–C_{60}	649	653	10.0	10.3	0.07	0.08	1.91	1.90
	H_2P–*$[Cu(phen)_2]^+$–C_{60}	–	777	–	–	$4.9x10^{-4}$	$1.1x10^{-3}$	–	1.60
13	*$[Cu(phen)_2]$–C_{60}[b]	765	–	–	–	$2.5x10^{-4}$	–	1.62	–
	$[Cu(phen)_2]$–*C_{60}[b]	710	–	0.1	–	$2.3x10^{-5}$	–	1.75	–
14	^{1}*MgP–$[Cu(phen)_2]^+$	619	613	5.1	6.3	0.06	0.06	2.00	2.02
	MgP–*$[Cu(phen)_2]^+$	–	775	–	–	$8.0x10^{-4}$	$1.1x10^{-3}$	–	1.60
15	*$[Cu(phen)_2]^+$	–	765	–	2.5	$4.8x10^{-3}$ [23]	–	–	1.62
16	^{1}*C_{60}–malonate[d]	715	–	1.48	–	$1.0x10^{-3}$	–	1.73	–

[a] Energy of the corresponding excited state relative to the ground state, calculated from the emission maximum (λ_{max}) [b]in dichloromethane, from ref 23; [c] in benzene, from ref 51; [d] in chloroform, from ref 23.

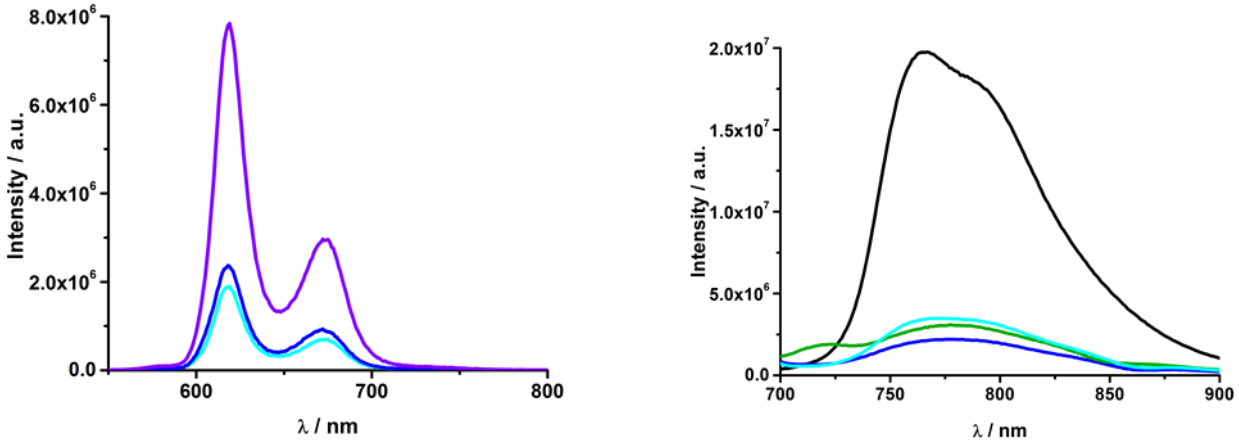

Fig.3 Left: emission spectra of MgP (violet) and catenates **11** (blue) and **14** (cyan) in THF upon excitation at 430 nm (OD = 0.075) at room temperature. Right: emission spectra of $[Cu(phen)_2]^+$ **15** (black) and catenates **11** (blue), **12** (olive) and **14** (cyan) in PhCN upon excitation at 320 nm (OD = 0.07) at room temperature.

latter amounts to about 20 % relative to reference **8**. In time-resolved emission experiments, lifetimes of 6.1 ns for **11**, 10.3 ns for **12** and 6.3 ns for **14** were determined in PhCN compared to 10.5 ns for **7** and 11.0 ns for **8**. Since the porphyrin emission is quenched not only in catenates **11** and **12**, but also in catenate reference **14**, which lacks C_{60}, we ascribe the underlying process to an EnT from either MgP or H_2P to $[Cu(phen)_2]^+$. Based on thermodynamics, ET is unlikely to happen between MgP/H_2P and $[Cu(phen)_2]^+$. Catenates **11**, **12**, and **14** were also excited at 320 nm, which coincides with the maximum absorption of $[Cu(phen)_2]^+$. The emission spectra with broad features between 730 and 860 nm are shown in Fig. 3. The MLCT emission quantum yields of catenates **11**, **12**, and **14** are on the order of 10^{-4}, which is approximately one order of magnitude smaller than that recorded for reference $[Cu(phen)_2]^+$ catenate **15** (Table 2). A possible rationale is a slow transduction of triplet excited state energy back to either MgP or H_2P. The weak fluorescence of C_{60} could not be probed in catenates **11** and **12**, due to strongly overlapping absorption and emission bands.

3.2. Singlet oxygen quantum yields. To gain further insight into photo-processes taking place in catenates **11**, **12**, and **14**, in particular intersystem crossing (ISC) to give triplet excited states, singlet oxygen quantum yields (Φ_Δ) were determined using porphyrin **8** in THF as a reference.[53,54] The results are summarized in Table 3. Compared to reference **8**, H_2P–$[Cu(phen)_2]^+$–C_{60} catenate **12** exhibits a nearly 50 % lower singlet oxygen phosphorescence – Fig. 4. Also MgP–$[Cu(phen)_2]^+$–C_{60} catenate **11** as well as MgP–$[Cu(phen)_2]^+$ catenate **14** show a quenched $^1O_2$ quantum yield compared to MgTPP – Table 3. It is clear that C_{60} plays an important role, since **11** displays even lower $^1O_2$ phosphorescence than does **14** – Fig. 4. Furthermore, MgP has a stronger inhibiting influence on the ISC than H_2P. From these results it is concluded that upon photoexcitation of catenates **11**, **12**, and **14**, alternative deactivation pathways are in competition with ISC. In particular, EnT and ET take place due to the presence of $[Cu(phen)_2]^+$ and C_{60}, respectively. Based on these experiments, energy transfer from $^{3*}[Cu(phen)_2]^+$ to ZnP, MgP or H_2P is ruled out, since this would have led to higher singlet oxygen quantum yields, which was not observed.

Table 3 Singlet oxygen quantum yields Φ_Δ

Compound	Solvent	Φ_Δ
7	benzene	0.66[53]
8	benzene	0.62[53,54]
	THF	0.62[54]
11	THF	0.24
12	THF	0.34
14	THF	0.32

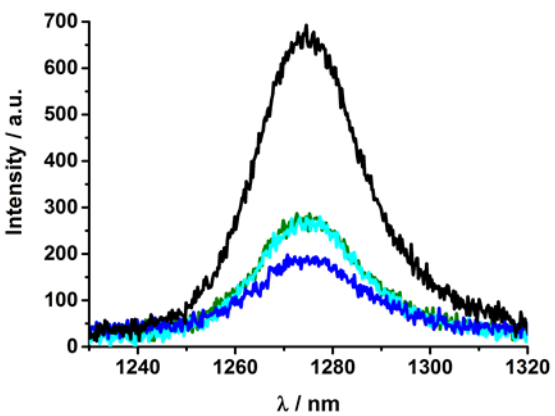

Fig.4 $^1O_2$ phosphorescence of 8 (black), catenates **11** (blue), **12** (olive) and **14** (cyan) in THF upon excitation at 347 nm (OD = 0.045) at room temperature.

Journal Name RSCPublishing

ARTICLE

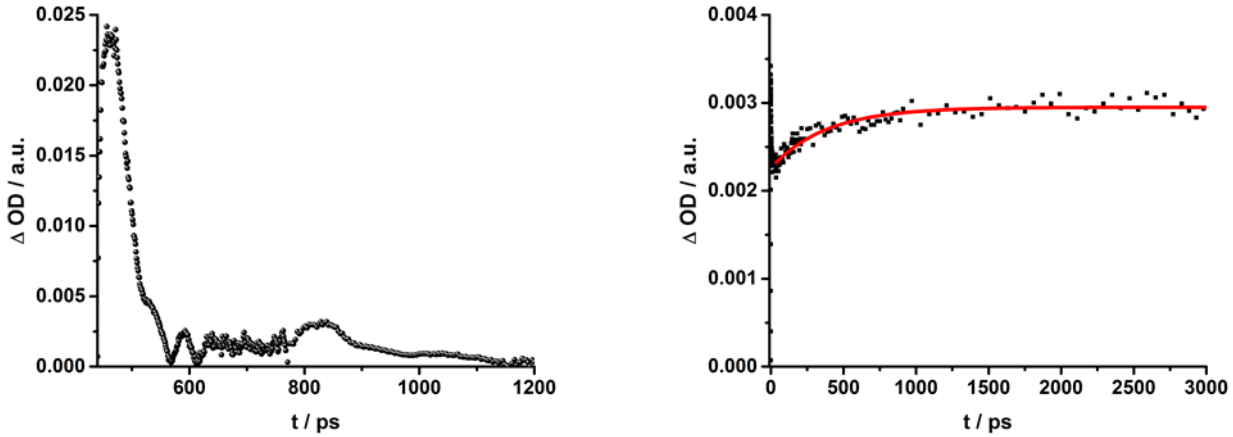

Fig.5 Left: Differential absorption spectrum (visible and near-infrared) registered upon femtosecond flash photolysis (420 nm, 150 nJ) of MgP reference **7** in THF with a time delay of 3.2 ns at room temperature. Right: time-absorption profile of MgP at 840 nm, monitoring the intersystem crossing process.

3.3 Transient absorption. To obtain information about the formation and deactivation processes taking place upon photoexcitation of catenates **11**-**15** and references **7**, **8**, and **16,** transient absorption studies were carried out. Upon 420 nm excitation of MgP reference **7**, characteristic differential absorption changes evolve immediately after the laser pulse in THF. An intense transient absorption is observed with a maximum at 460 nm, along with a broad absorption in the 580 to 750 nm range, which corresponds to the MgP singlet excited state (Fig. 5).[12] This absorption decays at a rate of 1 x 10^8 s^{-1} affording the energetically lower lying triplet excited state. The signature of the latter is a 840 nm absorption maximum,[55] which develops with kinetics similar to the decay of the MgP singlet absorption at 460 nm. Transient bleaching at 570 and 610 nm reflects the MgP Q-band absorption. It is discernible from Fig. 5 that the differential absorption spectra after a time delay of 3.2 ns exhibit feature characteristics of both the singlet and triplet excited states of MgP.

For C_{60}-malonate **16**, the differential absorption spectra in THF – Fig. 6 – show formation of the singlet excited state upon excitation at 387 nm with maxima at 510 and 920 nm, which then undergoes nearly quantitative intersystem crossing with a rate constant of 6 x 10^8 s^{-1} to give the energetically lower lying triplet excited state with a characteristic absorption maximum at 720 nm.[23,24] Fig. 6 portrays the kinetics of the intersystem crossing process. In complementary nanosecond experiments a triplet lifetime of 23 μs was determined in argon–saturated THF, comparable to the value of 20 μs measured in PhCN.[22]

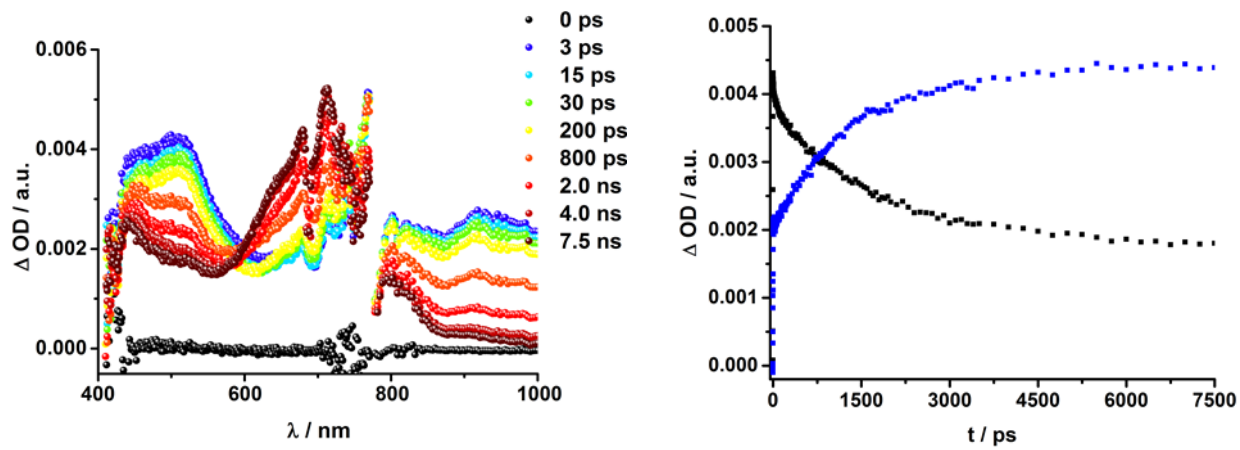

Fig.6 Left: differential absorption spectra (visible and near-infrared) registered upon femtosecond flash photolysis (387 nm, 200 nJ) of C_{60}-malonate **16** in THF with time delays between 0 and 7.5 ns at room temperature. Right: time-absorption profiles of C_{60}-malonate 7 at 510 nm (black) and 680 nm (blue), monitoring the intersystem crossing process.

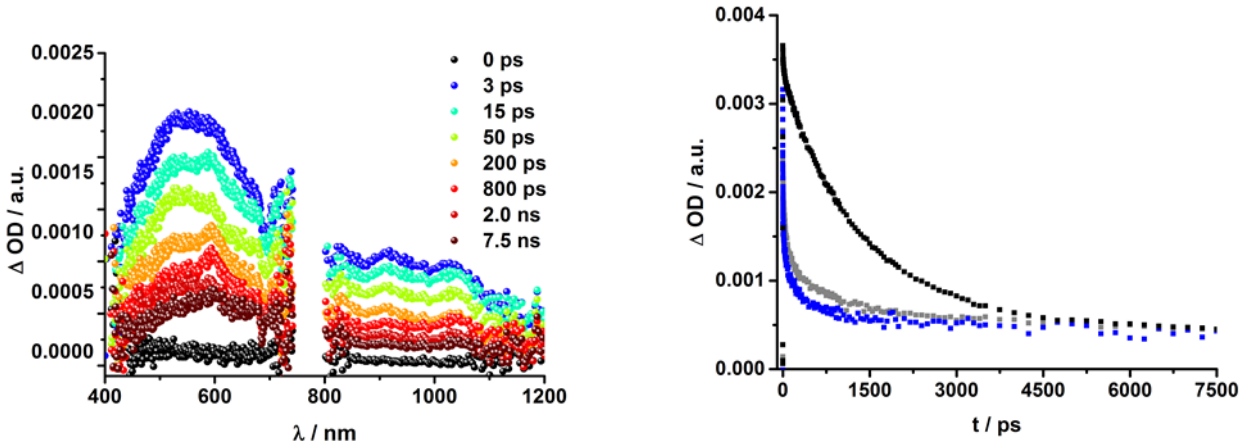

Fig.7 Left: Differential absorption spectra (visible and near-infrared) registered upon femtosecond flash photolysis (387 nm, 200 nJ) of $[Cu(phen)_2]^+$–C_{60} catenate reference **13** in THF at room temperature with time delays between 0 and 7.5 ns. Right: time-absorption profiles of catenates **11** (blue) and **13** (grey) as well as C_{60}-malonate **16** (black) at 920 nm, monitoring ET.

Upon excitation of $[Cu(phen)_2]^+$ reference catenate **15** at 387 nm in THF, the characteristic $[Cu(phen)_2]^+$ MLCT transient absorption is observed, which includes a broad maximum between 540 and 610 nm followed by another maximum around 910 nm.[20-24] Furthermore, minima at 440 and 700 nm correspond to the MLCT absorption. It is well established that the singlet excited MLCT state decays within hundreds of femtoseconds to yield the energetically lower lying MLCT triplet excited state.[56,57] Thus, the observed transient absorption is attributed to the MLCT triplet state, which has a lifetime of 645 ns under these conditions.[23]

Fig. 7 documents that following 387 nm excitation of $[Cu(phen)_2]^+$–C_{60} reference **13** in THF maxima at 530, 590, and 920 nm evolve, which is consistent with the results noted for reference compounds **15** and **16**. In contrast to C_{60}–malonate **16**, the excited state of **13** deactivates rapidly with a rate of 2.5×10^{10} s^{-1}, as a result of the close proximity between C_{60} and $[Cu(phen)_2]^+$. As seen for **15**, the triplet MLCT excited state does not decay completely within the time scale of our experimental setup of 7.5 ns. As a matter of fact, an additional peak is seen in the spectrum of catenate **13** at 1035 nm corresponding to the one-electron reduced form of C_{60},[33,55] indicating that the deactivation of the C_{60} singlet excited state of **13** involves ET. On the time scale of the femtosecond experiments, the C_{60} radical anion is stable. It was only on the time scale of complementary nanosecond experiments that a lifetime of 100 ns could be determined for the CSS of **13** in THF.

Upon excitation of MgP–$[Cu(phen)_2]^+$ reference catenate **14**, at either 387 or 420 nm, the differential absorption spectra are dominated by the MgP singlet excited state, due to the strong porphyrin absorption in this region. As seen for MgP reference **7**, a transient evolves in THF directly after laser excitation that features a maximum at 460 nm, broad transient absorption between 580 and 750 nm, and transient bleaching at 570 and 610 nm – compare Fig.s 5 and 8. In sharp contrast to the MgP reference, the singlet excited state of catenate **14** undergoes rapid EnT from the singlet excited state of MgP to the lower lying $[Cu(phen)_2]^+$ excited state, as determined by the decay at 460 nm, at a rate of 2.5×10^9 s^{-1} in THF (see Fig. 8). Nonetheless, this EnT process is not quantitative as the features of ^{3}MgP* are still discernible in the 480 to 840 nm region of Fig.7.

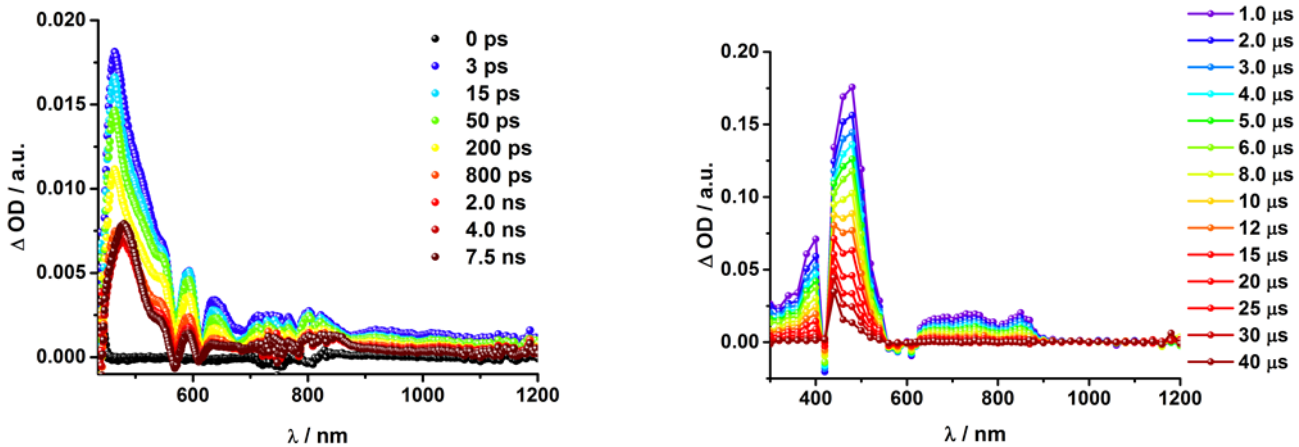

Fig.8 Left: differential absorption spectra (visible and near-infrared) registered upon femtosecond flash photolysis (387 nm, 200 nJ) of MgP–$[Cu(phen)_2]^+$ catenate **14** in THF with time delays between 0 and 7.5 ns at room temperature. Right: differential absorption spectra (visible and near infrared) registered upon nanosecond flash photolysis (355 nm, 10 mJ) of MgP–$[Cu(phen)_2]^+$ catenate **14** in THF with time delays between 1 and 40 µs at room temperature.

In addition to the MgP excited states, the transient absorption corresponding to the MLCT triplet excited state is detected at ~ 950 nm, which decays within 660 ps. In the visible region of the spectrum, the MLCT features are obscured by the much stronger

MgP transients. Turning to the nanosecond transient absorption spectra in Fig. 8, right, only the long-lived (15.8 μs) features of ^{3}MgP* are discernible in the visible region. We note that the ^{3}MLCT* features could not be clearly identified in these spectra because of their comparably small extinction coefficients and shorter lifetimes, on the order of hundreds of nanoseconds.

MgP–[Cu(phen)$_2$]$^+$–C$_{60}$ and H$_2$P–[Cu(phen)$_2$]$^+$–C$_{60}$ catenates **11** and **12** were also excited at 387 as well as 420 nm in THF and PhCN. As seen in the aforementioned references the differential absorption spectra are dominated by the fingerprints of MgP and H$_2$P. For example, in catenate **11** upon selective excitation of MgP with a 420 nm laser pulse, maxima are observed at 465, 590, and 640 nm and transient bleaching is seen at 570 and 610 nm. All of these features correspond to the MgP singlet excited state (Fig. 9). In analogy to **14**, we again observe a faster decay of the MgP singlet excited state than seen for reference **7,** consistent with EnT to [Cu(phen)$_2$]$^+$. Upon 387 nm excitation of **11,** the features of the C$_{60}$ singlet excited state develop at 920 nm. Unlike C$_{60}$ reference **16**, the C$_{60}$ singlet excited state deactivates in **11** rapidly – Fig. 7 – to yield the one electron reduced form of C$_{60}$ with its characteristic absorption at 1035 nm.[56,57] This species was stable throughout the 7.5 ns time scale of our experimental setup. In the visible region, the MgP singlet and triplet state absorption again mask the MLCT excited states. To gain insight into the back ET process, catenate **11** was excited with a 6 ns laser pulse at 355 and 532 nm. Regardless of selectively exciting MgP at 532 nm or unselectively exciting all components at 355 nm, the visible region of the differential absorption spectra is dominated by the triplet excited state features of MgP, with maxima at 470 and 840 nm (see Fig. 10). Furthermore, the 680 and 720 nm maxima, which are clearly observed in Fig. 10, correspond to the one electron oxidized form of MgP and the triplet excited state of C$_{60}$, respectively. Since the spectroscopic signatures of the latter two overlap with each other as well as with that of MgP triplet excited state, the signature absorption for the one electron oxidized form of MgP becomes evident only upon quenching of the MgP and C$_{60}$ triplet excited states by molecular oxygen. This is documented in Fig.s 10 and 11. A biexponential fit of the decay at 680 nm in the presence of oxygen yields a short-lived component of 190 ns and a long-lived component of 700 ns. The former relates to quenched C$_{60}$ triplet excited states, while the latter correlates with the one electron oxidized form of MgP. A closer look at the near infrared region allows identification at shorter times of the fingerprint absorption of the one electron reduced form of C$_{60}$ at 1035 nm – Fig. 10. The 1035 nm decay follows a biexponential rate law with lifetimes of 60 and 700 ns in THF in the absence as well as the presence of oxygen. The shorter lifetime resembles that found for CSS in reference catenate **13** and is ascribed to the close MgP-[Cu(phen)$_2$]$^{2+}$-C$_{60}^{\bullet-}$ CSS. The fact that the shorter lifetime seen for **11** (60 ns) is less than that of **13** (100 ns) indicates that there is an additional deactivation pathway for the close CSS in catenate **11** when MgP is present, namely a charge shift from MgP to the oxidized Cu ion. The longer lifetime of 700 ns observed with **11** matches the lifetime found for the one electron oxidized form of MgP, and is assigned to the long distance MgP$^{\bullet+}$–[Cu(phen)$_2$]$^+$–C$_{60}^{\bullet-}$ CSS. Clearly, back ET in catenate **11,** although exergonic, is inhibited due to the spatial separation of the oxidized donor and the reduced acceptor and the fact that the process is in the Marcus inverted region.

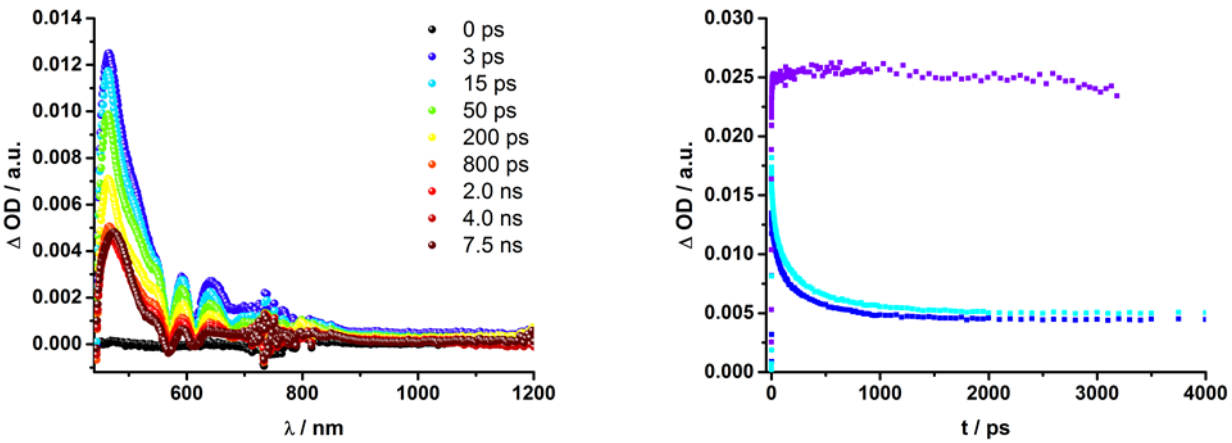

Fig.9 Left: differential absorption spectra (visible and near-infrared) registered upon femtosecond flash photolysis (420 nm, 150 nJ) of MgP-[Cu(phen)$_2$]$^+$-C$_{60}$ catenate **11** in THF with time delays between 0 and 7.5 ns at room temperature. Right: time-absorption profiles of catenates 11 (blue) and 14 (cyan) as well as MgP (violet) at 465 nm, monitoring EnT.

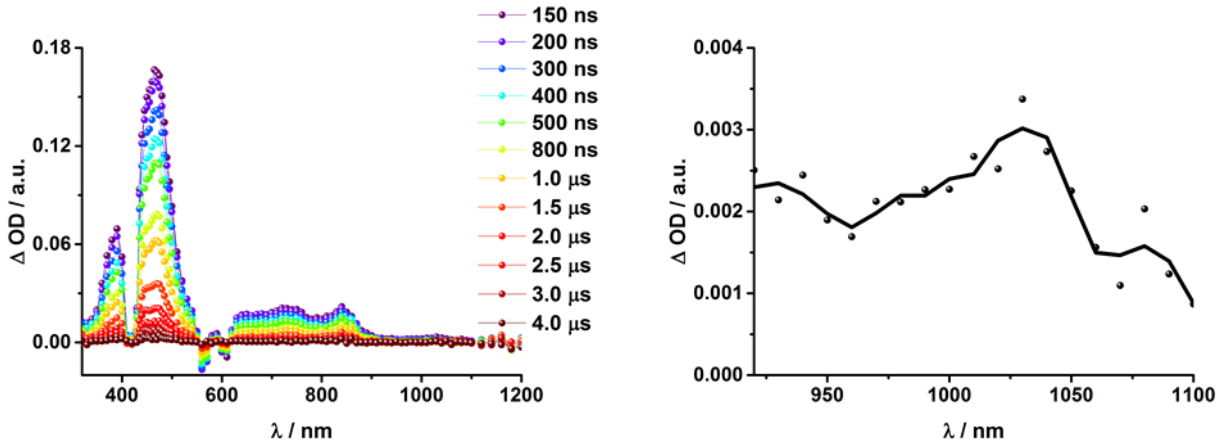

Fig.10 Left: transient absorption spectra (visible and near-infrared) observed upon ns flash photolysis (532 nm, 10 mJ) of MgP–$[Cu(phen)_2]^+$–C_{60}-catenate **11** in THF with time delays between 150 ns and 4.0 µs at room temperature under aerobic conditions. Right: transient absorption spectrum (near-infrared) observed upon ns flash photolysis (532 nm) of MgP-$[Cu(phen)_2]^+$-C_{60}-catenate 11 in THF with a time delay of 150 ns at room temperature under aerobic conditions.

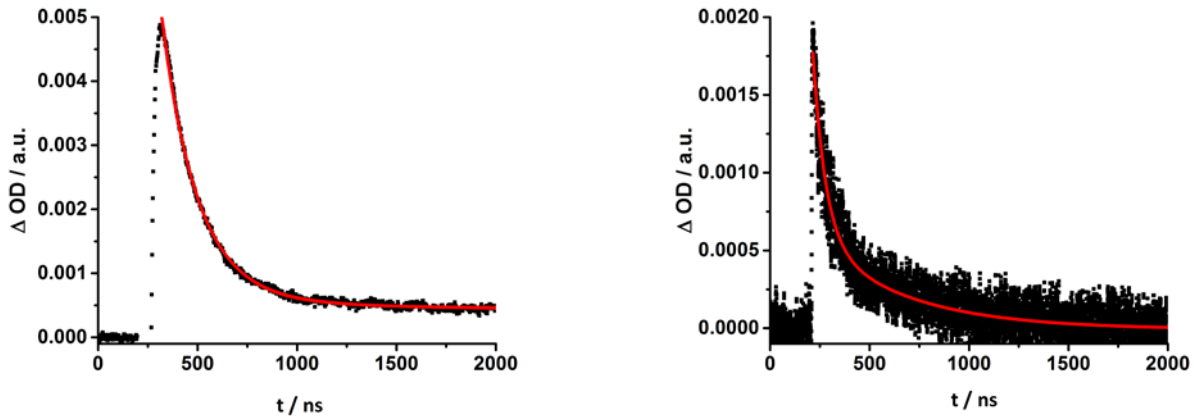

Fig.11 Left: time-absorption profile observed upon nanosecond flash photolysis (355 nm) of MgP– $[Cu(phen)_2]^+$–C_{60} catenate **11** in THF at 680 nm in THF saturated with molecular oxygen, monitoring back ET. Right: time-absorption profile observed upon nanosecond flash photolysis (355 nm) of MgP–$[Cu(phen)_2]^+$–C_{60}-catenate **11** in THF at 1030 nm under aerobic conditions, monitoring back ET.

From the transient absorption spectra of H_2P-$[Cu(phen)_2]^+$-C_{60} catenate **12** a similar reaction pattern is derived. Excitation at 420 nm is followed by the immediate formation of the H_2P singlet excited state with maxima at 450, 540, 570, 620, and 680 nm as well as a broad transient absorption between 1000 – 1150 nm. These features are stable on the time scale of our experimental setup of 7.5 ns. Additionally, ground state bleaching at 420, 520, 550, 590, and 650 nm is seen, corresponding to the Soret- and Q-band absorption of H_2P. Fig. 12 shows that upon excitation of **12** at 387 nm the transient absorption of the C_{60} singlet excited state is also observed in the region between 850 and 1000 nm. However, assignment of CSS involving the one electron oxidized form of H_2P at 680 nm and the one electron reduced form of C_{60} at 1035 nm is hampered in these femtosecond experiments by the much stronger H_2P excited state features. Only, in complementary nanosecond experiments is the absorption at 1035 nm clearly identified upon excitation at 355 nm as well as 532 nm – Fig. 13. Taking a closer look at the kinetics of the 1035 nm decay in THF – Fig. 14 – lifetimes of 20 and 400 ns are derived. Similarly, the decay at 680 is fit with a lifetime of 400 ns in THF in oxygen-saturated solution. Analogously to catenate **11**, the longer lifetime for **12** correlates with the distant $H_2P^{\bullet+}$-$[Cu(phen)_2]^+$-$C_{60}^{\bullet-}$ CSS, while the shorter lifetime is assigned to the close H_2P–$[Cu(phen)_2]^{2+}$–$C_{60}^{\bullet-}$ CSS.

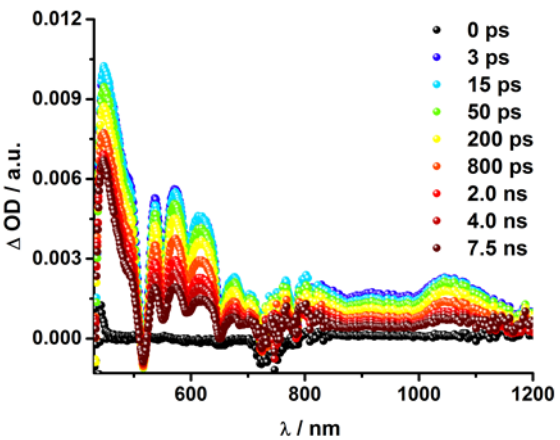

Fig.12 Differential absorption spectra (visible and near-infrared) registered upon femtosecond flash photolysis (387 nm, 200 nJ) of H_2P–$[Cu(phen)_2]^+$–C_{60} catenate **12** in THF with time delays between 0 and 7.5 ns at room temperature.

Journal Name RSCPublishing

ARTICLE

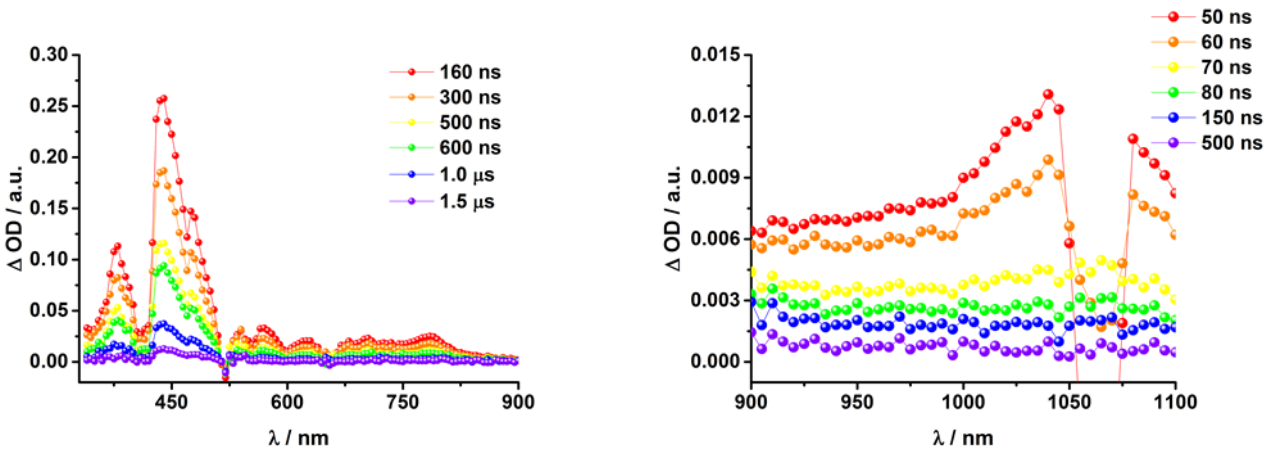

Fig.13 Top: differential absorption spectra (visible and near-infrared) registered upon femtosecond flash photolysis (532 nm, 10 mJ) of H_2P–$[Cu(phen)_2]^+$–C_{60} catenate **12** in THF with time delays between 120 ns and 1.5 µs at room temperature. Bottom: differential absorption spectra (visible and near-infrared) registered upon femtosecond flash photolysis (532 nm, 10 mJ) of H_2P–$[Cu(phen)_2]^+$–C_{60} catenate **12** in THF with time delays between 50 ns and 500 ns at room temperature.

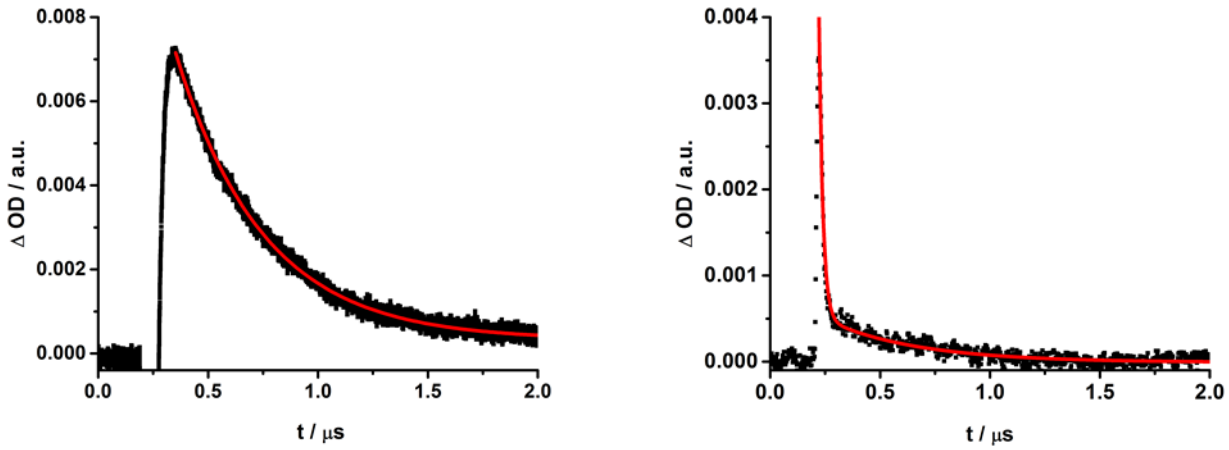

Fig.14 Time–absorption profiles of the spectra in Fig. 13 at 690 nm (left) and 1035 nm (right), monitoring back ET.

3.4 Efficiency of ET. Transient absorption measurements have clearly proven that MgP– and H_2P–$[Cu(phen)_2]^+$–C_{60} catenates **11** and **12** undergo ET upon photoexcitation. Their ZnP analog **10** is known from our earlier work[23] to form a long lived CSS. However, steady state experiments suggest that the efficiency for ET in these three porphyrin–C_{60} catenates is not the same. Redox potentials derived from electrochemical data imply a reduced driving force for the electron transfer in **12** and an enhanced driving force for **11** compared to **10** – Tables 1 and 4. Fluorescence quantum yields – Table 2 – underline this trend. In **12**, the porphyrin fluorescence is only 30 % quenched compared to that of the H_2P reference **8**, while in **11** the porphyrin fluorescence is over 60 % lower than that of MgP reference **7**; ZnP catenate **10** shows fluorescence quenching of 75 % compared to a ZnP reference.[23] Furthermore, the quantum yields for singlet oxygen formation Φ_Δ is almost 50 % lower for **12** compared to **8**, whereas for MgP catenate **11** Φ_Δ is more than 60 % lower than that of MgP reference **7**.

To find out more about the efficiency of the ET process, ns transient absorption was carried out with catenates **10**, **11**, and **12** under exactly the same conditions and the C_{60} radical anion absorption in the NIR region for each catenate was compared with respect to its intensity at the maximum – Fig. 15. In line with the predictions made from the steady state experiments, **10** clearly shows the strongest C_{60} anion signature absorption. Catenates **11** and **12** exhibited considerably weaker $C_{60}^{\bullet-}$ absorptions, namely 54% and 74% relative to **10**, which is in agreement with the weaker quenched porphyrin fluorescence. Those findings can be rationalized taking the driving forces for the ETs in the different catenates into account (Table 4).

Journal Name RSCPublishing

ARTICLE

Table 4 Charge separated state lifetimes and driving forces for ET of the porphyrin-C_{60} catenates.

Compound		Solvent	CSS Lifetimes in ns		Driving force in eV	
			close	distant	close	distant
ZnP–$[Cu(phen)_2]^+$–C_{60}[23]	**10**	PhCN	15	1060	0.81	0.81
MgP–$[Cu(phen)_2]^+$–C_{60}	**11**	THF	60	700	0.59	0.87
H_2P–$[Cu(phen)_2]^+$–C_{60}	**12**	THF	20	400	0.59	0.46
$[Cu(phen)_2]^+$–C_{60}	**13**	THF	100	-	0.47	-

The largest driving force to form the close CSS was found for **10** (0.81 eV), compared to 0.59 eV for **11** and **12** (for further discussion, see summary and conclusions).

Table 4 summarizes the CSS lifetimes of the investigated catenates **11**, **12**, and **13** as well as ZnP–$[Cu(phen)_2]^+$–C_{60} **10**, which we previously reported.[23] When comparing the three P–$[Cu(phen)_2]^+$ –C_{60} catenates, the influence of the metalloporphyrin on the charge separated states becomes evident. Catenate **11** reveals the longest lifetime for the close P–$[Cu(phen)_2]^{2+}$–$C_{60}^{\bullet-}$ charge separated state, while its ZnP analog **10** exhibits the longest lifetime for the long distance $P^{\bullet+}$–$[Cu(phen)_2]^+$–$C_{60}^{\bullet-}$ CSS.

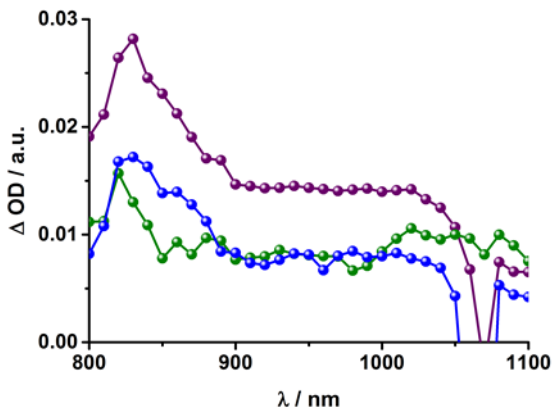

Fig.15 Differential absorption spectra (visible and near–infrared) registered upon nanosecond flash photolysis (532 nm, 10 mJ) of catenates **10** (purple), **11** (blue) and **12** (olive) in THF at room temperature under aerobic conditions.

Summary and Conclusions

In this work, we have demonstrated that a sequence of EnT and ET processes upon photoexcitation of MgP catenane **11** and H_2P catenate **12**. In particular, upon 420 nm excitation of the porphyrins, their singlet excited states are formed with energies of about 2 eV relative to the ground state (see Table 2 and Fig. 16). From these singlet excited states, deactivation processes occur via the energetically lower lying triplet excited states of either the porphyrin (~1.5 eV) or the copper–phenanthroline complex (~1.6 eV). The porphyrin triplet excited state decays directly back to the ground state, while ET evolves from the $[Cu(phen)_2]^+$ triplet excited MLCT state. In both catenates, the close P-$[Cu(phen)_2]^{2+}$–$C_{60}^{\bullet-}$ CSS is first formed with an oxidized Cu ion. Subsequent charge shift yields the distant $P^{\bullet+}$–$[Cu(phen)_2]^+$–$C_{60}^{\bullet-}$ CSS. In catenane **11**, the oxidation potential for MgP is lower than that of $[Cu(phen)_2]$, which leads to a lower lying distant $MgP^{\bullet+}$–$[Cu(phen)_2]^+$–$C_{60}^{\bullet-}$ CSS (1.14 eV), compared to the close CSS (1.42 eV). In turn, the charge shift is thermodynamically downhill. Evidence for the involvement of both states comes from the back ET dynamics.

The decay kinetics of the C_{60} radical anion at 1030 nm (Fig. 11) requires a biexponential fit, yielding lifetimes of 60 ns (k = 5.0 x 10^7 s^{-1}) and 700 ns (k = 2.5 x 10^6 s^{-1}). The faster decay is assigned to back ET in the MgP-$[Cu(phen)_2]^{2+}$–$C_{60}^{\bullet-}$ CSS, since the dynamics resemble those seen in reference catenate **13**. The longer lifetime matches the lifetimes determined for the single oxidized MgP and is, thus, assigned to back ET of the $MgP^{\bullet+}$–$[Cu(phen)_2]^+$–$C_{60}^{\bullet-}$ CSS. For catenane **12**, the redox potentials – Table 2 – suggest that the close CSS is energetically lower that the distant CSS, namely 1.32 eV compared to 1.45 eV. In spite of that, the charge shift to afford the distant $H_2P^{\bullet+}$-$[Cu(phen)_2]^+$–$C_{60}^{\bullet-}$ CSS seems to take place. Kinetic evidence comes from the biexponential decay of the C_{60} radical anion fingerprint – Fig. 14. Nevertheless, the pre-exponential factors for the short lifetime of 20 ns for the close CSS is 10^6 times larger than for the longer lifetime of 400 ns for the distant CSS. This gives rise to the conclusion that only a small portion of H_2P-$[Cu(phen)_2]^+$–C_{60} catenanes **12** undergoes charge shift to yield the distant CSS.

Fig. 16 schematically depicts the sequence of photoinduced processes and the energy levels determined from electrochemical and spectroscopic investigations together with the back ET dynamics from our newly investigated catenanes **11** and **12** as well as the previously studied catenate **10**.[23] At first glance, compared to the previously studied ZnP–$[Cu(phen)_2]^+$–C_{60} catenane **10**[23], in which both close and distant CSS appear to be isoenergetic, faster back ET was observed in both of the newly studied systems. H_2P–$[Cu(phen)_2]^+$–C_{60} catenane **12** has the shortest CSS lifetime (400 ns) of the three structurally similar catenated materials, which can be rationalized by the higher oxidation potential of H_2P and, in

Journal Name RSCPublishing

ARTICLE

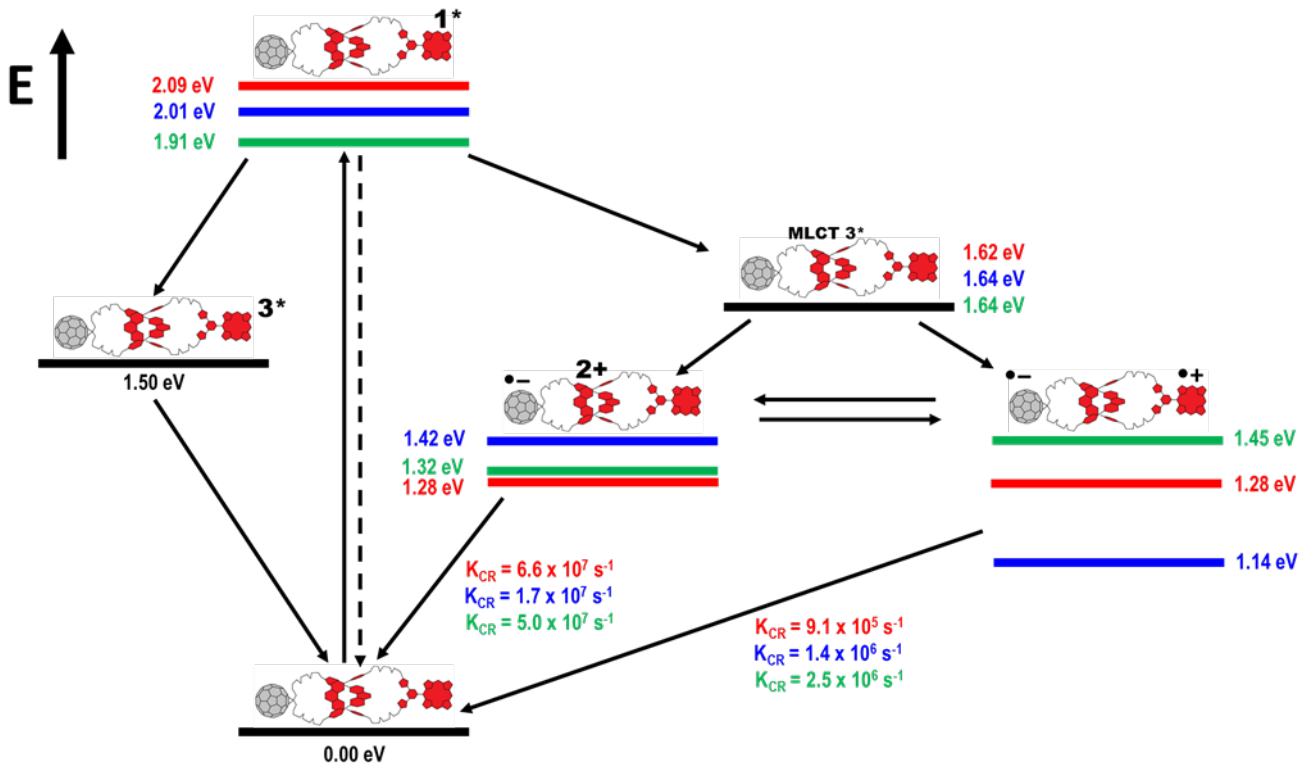

Fig.16 Schematic energy level diagrams, proposed decay pathways and rate constants for P-Cu^{+}-C_{60} catenates **10**[23] (red numbers), **11** (blue numbers) and **12** (green numbers) upon excitation at 420 nm. k_{CR} = charge recombination rate.

turn, decreased driving force for electron (charge) transfer. On the other hand, the relatively low oxidation potentials of MgP suggest an increased driving force for electron (charge) transfer. A closer look at the ET driving forces reveals, however, that the differences are more distinct. For example, the driving force to form the close CSS in **11** and **12** are identical, 0.59 eV, and considerably smaller than the 0.81 eV seen for **10**.[23] Considering that H_2P in **12** is harder to oxidize (0.38 V; Table 1) than ZnP in **10** and MgP in **11,** and that **12** also features the lowest singlet excited state energy (1.91 eV; Table 2) among these three, the ET driving force is nonetheless reduced in catenate **12**. Although MgP is more susceptible towards oxidation than H_2P and ZnP, **11** does not possess the largest driving force, since its singlet excited state energy is lower than that for **10**. Moreover, the close MgP–$[Cu(phen)_2]^{2+}$–$C_{60}^{\bullet-}$ CSS has a higher energy than ZnP–$[Cu(phen)_2]^{2+}$–$C_{60}^{\bullet-}$ and H_2P–$[Cu(phen)_2]^{2+}$–$C_{60}^{\bullet-}$. As a matter of fact, the latter numbers are in sound agreement with the efficiency results in terms of ET to afford the close CSS, namely **10** > **11** > **12**. The energy levels for the distant CSS give a slightly different picture. In **12**, the charge shift is very unlikely to occur, since the distant CSS is of higher energy (1.45 eV) than the close CSS (1.32 eV). This is also reflected in the transient absorption spectra and the corresponding kinetics – see Fig.s 13 and 14. Here, much higher intensities evolve for the close CSS with its 20 ns lifetimes than for the distant CSS. In **12**, the latter is highest in energy relative to **10** and **11** and gives rise to the shortest lifetime with 400 ns. In **11**, the charge shift is downhill with a driving force of 0.87 eV. Finally, in **10**, in which both close and distant CSS have the same energy (1.28 eV)[23], exhibits a comparable driving force of 0.81 eV. Still, ET occurs most efficiently in **10** despite the slowest charge recombination rate.

Based on the aforementioned considerations, we analyzed the dynamics for all charge separation, charge shift and charge recombination processes for the close and distant CSS, respectively, with the Marcus formalism,[30] from which we derived reorganization energies of 0.57 eV for the close CSS and 0.67 eV for the distant CSS, respectively.

From those results we conclude that the initial EnT from the porphyrin to the $[Cu(phen)_2]^{+}$ is the efficiency determining step. ZnP in **10** exhibits the highest lying singlet excited state (2.09 eV), the strongest fluorescence quenching of ~ 75 %, and the shortest lived singlet excited state (0.5 ns; see Table 2). In stark contrast, in **11** and **12** the MgP and H_2P fluorescence is only quenched about 60 % and 30 %, respectively. Thus, EnT from the ZnP singlet excited state to $[Cu(phen)_2]^{+}$ (1.6 eV) is more efficient than from the MgP singlet excited state (2.01 eV) and the H_2P singlet excited state (1.91 eV). Consequently, **10** undergoes a more efficient subsequent ET. Additionally, the initial ET to afford the close CSS seems to play an important role. The driving forces determined for this process reflect the tendency seen for the efficiency of the ET and also the lifetimes

for the distant CSS, namely that ET in **10** is most efficient and back ET is slowest (9.1×10^5 s^{-1})[23].

In summary, it has been shown that replacing ZnP with MgP or H_2P in $[Cu(phen)_2]^{2+}$–C_{60} catenates does not enhance ET processes or give longer lived CSS. Nevertheless, we demonstrated that MgP–$[Cu(phen)_2]^{+}$–C_{60} **11** as well as MgP–$[Cu(phen)_2]^{+}$–C_{60} **12** undergo EnT as well as ET followed by a charge shift to form the long lived radical ion pair $P^{\bullet+}$–$[Cu(phen)_2]^{+}$–$C_{60}^{\bullet-}$ with lifetimes of hundreds of nanoseconds. The comprehensive photophysical and electrochemical characterization of the catenates and their references yielded a useful set of thermodynamic and kinetic data. Thus, critical comparison with the previously studied ZnP analog provided new insights into the effects of the porphyrin metal center (or the lack of it) on ET dynamics in mechanically interlocked artificial photosynthetic model systems.

Experimental Section

General Information and Materials. NMR spectra were obtained on either a Bruker AVANCE 400 (400 MHz) or an AVANCE 800 (800 MHz) spectrometer using deuterated solvents as the lock. The spectra were collected at 25 °C, and chemical shifts (δ, ppm) were referenced to residual solvent peak. In the assignments, the chemical shift (in ppm) is given first, followed, in parentheses, by multiplicity (s, singlet; d, doublet; t, triplet; m, multiplet; br, broad), the number of protons implied and finally the assignment. In the ^{1}H NMR assignment (δ), H_o and H_m refer to the hydrogen atoms at the *ortho* and *meta* positions, respectively, of the phenyl ring attached to the phenanthroline ring system, whose hydrogen atoms are numbered $H_{3,8}$, $H_{4,7}$ and $H_{5,6}$, respectively. ZnP, MgP and H_2P are used as abbreviations for zinc(II)porphyrin, magnesium(II)porphyrin and free-base porphyrin, respectively. MALDI-TOF mass spectra were recorded in a Bruker Omni FLEX MALDI-TOF MS spectrometer. This instrument was operated at an accelerating potential of 20 kV in linear mode. The mass spectra represent an average over 256 consecutive laser shots. The mass scale was calibrated using the matrix peaks and the calibration software available from Bruker OmniFLEX. Mentioned *m*/*z* values correspond to monoisotopic masses. The compound solutions (10^{-3} mol/L) were prepared in THF. The matrix, α-cyano-4-hydroxycinnamic acid (CCA), was purchased from Aldrich and used without further purification, while 1,4 benzoquinone (BQ), also from Aldrich, was recrystallized from ethanol before use. BQ was used as matrix for magnesium containing compounds, whereas CCA was employed for all other compounds. The appropriate matrix was dissolved (10 g/L) in a solvent mixture composed of H_2O/CH_3CN/TFA (25/75/1, v/v). Two microliters of compound solution was mixed with 10 μL of matrix solution. The final solution was deposited onto the sample target and allowed to dry in air. All chemicals were purchased from Sigma-Aldrich and Alfa Aesar and used without further purification. For moisture-sensitive reactions, solvents were freshly distilled. Methylene chloride (CH_2Cl_2) and acetonitrile (CH_3CN) were dried over calcium hydride while tetrahydrofuran (THF) was dried using sodium/benzophenone. Anhydrous dimethylformamide (DMF) was used as received. All syntheses were carried out using Schlenk line techniques. Moisture-sensitive liquids were transferred by cannula or syringe. The progress of the reactions was monitored by thin-layer chromatography (TLC) whenever possible. TLC was performed using precoated glass plates (silica gel 60, 0.25 mm thickness) containing a 254 nm fluorescent indicator. Column chromatography was carried out using Merck silica gel 60 (0.063-0.200 mm) and neutral alumina (Brockmann I, activated, 150 mesh, 58 Å).

Synthesis. Building blocks **1**, **2** and **3** as well as porphyrin derivatives **6** and **8** were prepared according to our previous published reports. Porphyrin **7** and the fullerene model compound **16** were afforded as described in the literature.[23] All of the [2]catenates reported were synthesized from the suitable precursors following the general procedure for preparation of catenates described in our previous work.[20-25,45,46]

[2]Catenate 10 was synthesized from precursor **4** and porphyrin **6**. Final purification was achieved by column chromatography (SiO_2) using a gradient of CH_2Cl_2/CH_3OH (99:1 v/v) as eluent, affording **10** as a greenish purple solid (0.078 g, 57% yield). ^{1}H NMR (CD_3CN), δ ppm: 8.98 (s, 1H, H_a); 8.77 (d, 4H, pyrrolic protons); 8.69 (d, 2H, pyrrolic protons); 8.57 (d, 2H, pyrrolic protons); 8.45 (dd, 4H, $H_{4'}$, $H_{7'}$, H_4, and H_7); 8.11 (s, 2H, H_b); 7.85 (s, 6H, H_c on ZnP *tert*-butylphenyl groups); 7.81 (s, 2H, H_d); 7.80 (s, 2H, $H_{5'}$ and $H_{6'}$); 7.79 (s, 2H, H_5 and H_6); 7.64 (d, 2H, $H_{3'}$ and $H_{8'}$); 7.63 (s, 3H, H_e on ZnP-*tert*-butylphenyl group); 7.36 (d, 2H, H_3 and H_8); 7.07 (d, 4H, $H_{o'}$); 6.74 (d, 4H, H_o); 5.82 (d, 4H, $H_{m'}$); 5.67 (d, 4H, H_m); 5.04 (s, 4H, H_f); 4.69 (s, 4H, H_g); 4.80-3.00 (m, oligo(ethylene glycol) linker); 1.54 (s, 54H, *tert*butyl CH_3 groups). MALDI-TOF: *m*/*z* found 3216.1205 $[M - PF_6]^+$, calcd 3216.0098 for $C_{207}H_{152}N_{14}O_{16}ZnCu$.

[2]Catenate 11 was synthesized from precursor **4** and porphyrin **7**. Final purification was achieved by column chromatography (SiO_2) using a gradient of CH_2Cl_2/CH_3OH (99:1 v/v) as eluent, affording **11** as a greenish purple solid (0.072 g, 55% yield). ^{1}H NMR (CD_3CN), δ ppm: 8.95 (s, 1H, H_a); 8.70 (d, 4H, pyrrolic protons); 8.62 (d, 2H, pyrrolic protons); 8.56 (d, 2H, pyrrolic protons); 8.46 (dd, 4H, $H_{4'}$, $H_{7'}$, H_4, and H_7); 8.14 (s, 2H, H_b); 7.83 (s, 6H, H_c on MgP *tert*-butylphenyl groups); 7.80 (s, 2H, H_d); 7.78 (s, 2H, $H_{5'}$ and $H_{6'}$); 7.76 (s, 2H, H_5 and H_6); 7.66 (d, 2H, $H_{3'}$ and $H_{8'}$); 7.61 (s, 3H, H_e on MgP-*tert*-butylphenyl group); 7.37 (d, 2H, H_3 and H_8); 7.06 (d, 4H, $H_{o'}$); 6.75 (d, 4H, H_o); 5.84 (d, 4H, $H_{m'}$); 5.69 (d, 4H, H_m); 5.03 (s, 4H, H_f); 4.70 (s, 4H, H_g); 4.80-3.00 (m, oligo(ethylene glycol) linker); 1.59 (s, 54H, *tert*butyl CH_3 groups). MALDI-TOF: *m*/*z* found 3176.2091 $[M - PF_6]^+$, calcd 3176.0657 for $C_{207}H_{152}N_{14}O_{16}MgCu$.

[2]Catenate 12 was synthesized from precursor **4** and porphyrin **8**. Final purification was achieved by column chromatography (SiO_2) using a gradient of CH_2Cl_2/CH_3OH (98:2 v/v) as eluent, affording **12** as a purple solid (0.075 g, 58% yield). ^{1}H NMR (CD_3CN), δ ppm: 8.97 (s, 1H, H_a); 8.78 (d, 4H, pyrrolic protons); 8.73 (d, 2H, pyrrolic protons); 8.68 (d, 2H, pyrrolic protons); 8.48 (dd, 4H, $H_{4'}$, $H_{7'}$, H_4, and H_7); 8.15 (s, 2H, H_b); 7.89 (s, 6H, H_c on H_2P *tert*-butylphenyl groups); 7.83 (s, 2H, H_d); 7.77 (s, 2H, $H_{5'}$ and $H_{6'}$); 7.74 (s, 2H, H_5 and H_6); 7.69 (d, 2H, $H_{3'}$ and $H_{8'}$); 7.65 (s, 3H, H_e on H_2P-*tert*-butylphenyl group); 7.38 (d, 2H, H_3 and H_8); 7.05 (d, 4H, $H_{o'}$); 6.72 (d, 4H, H_o); 5.88 (d, 4H, $H_{m'}$); 5.70 (d, 4H, H_m); 5.03 (s, 4H, H_f); 4.73 (s, 4H, H_g); 4.80-3.00 (m, oligo(ethylene glycol) linker); 1.65 (s, 54H, *tert*butyl CH_3 groups). MALDI-TOF: *m*/*z* found 3154.5001 $[M - PF_6]^+$, calcd 3154.0963 for $C_{207}H_{154}N_{14}O_{16}Cu$.

[2]Catenate 13. This model compound was synthesized from precursor **4** and compound **9**. Final purification was achieved by column chromatography (SiO_2) using a gradient of CH_2Cl_2/CH_3OH (99:1 v/v) as eluent, affording **13** as a brown solid (0.071 g, 75% yield). ^{1}H NMR ($CDCl_3$), δ ppm: 8.88 (s, 1H, H_a); 8.42 (dd, 4H, pyrrolic protons); 8.73 (d, 2H, pyrrolic protons); 8.68 (d, 2H, pyrrolic protons); 8.48 (dd, 4H, $H_{4'}$, $H_{7'}$, H_4, and H_7); 8.13 (s, 2H, H_b); 7.81 (s, 2H, H_d); 7.80 (s, 2H, $H_{5'}$ and $H_{6'}$); 7.79 (s, 2H, H_5 and H_6); 7.64 (d, 2H, $H_{3'}$ and $H_{8'}$); 7.36 (d, 2H, H_3 and H_8); 7.07 (d, 4H, $H_{o'}$); 6.74 (d, 4H, H_o); 5.82 (d,

4H, $H_{m'}$); 5.67 (d, 4H, H_m); 5.04 (s, 4H, H_f); 4.69 (s, 4H, H_g); 4.80-3.00 (m, oligo(ethylene glycol) linker); 2.46 (s, 3H, CH_3 group). MALDI-TOF: *m/z* found 2295.2099 [M – PF_6]$^+$, calcd 2295.5363 for $C_{146}H_{84}N_{10}O_{16}Cu$.

[2]Catenate 14. This model compound was synthesized from precursor **5** and porphyrin **7**. Final purification was achieved by column chromatography (SiO_2) using a gradient of CH_2Cl_2/CH_3OH (98:2 v/v) as eluent, affording **14** as a greenish purple solid (0.065 g, 68% yield). ^{1}H NMR ($CDCl_3$), δ ppm: 8.96 (s, 1H, H_a); 8.74 (d, 4H, pyrrolic protons); 8.60 (d, 2H, pyrrolic protons); 8.54 (d, 2H, pyrrolic protons); 8.45 (dd, 4H, $H_{4'}$, $H_{7'}$, H_4, and H_7); 8.16 (s, 2H, H_b); 7.82 (s, 6H, H_c on MgP *tert*-butylphenyl groups); 7.81 (s, 2H, H_d); 7.78 (s, 2H, $H_{5'}$ and $H_{6'}$); 7.75 (s, 2H, H_5 and H_6); 7.68 (d, 2H, $H_{3'}$ and $H_{8'}$); 7.60 (s, 3H, H_e on MgP-*tert*-butylphenyl group); 7.38 (d, 2H, H_3 and H_8); 7.06 (d, 4H, $H_{o'}$); 6.73 (d, 4H, H_o); 5.84 (d, 4H, $H_{m'}$); 5.69 (d, 4H, H_m); 4.77 (s, 4H, H_g); 4.80-3.00 (m, oligo(ethylene glycol) linker); 1.58 (s, 54H, *tert*butyl CH_3 groups). MALDI-TOF: *m/z* found 2328.3825 [M – PF_6]$^+$, calcd 2328.0548 for $C_{142}H_{148}N_{14}O_{12}MgCu$.

[2]Catenate 15. This model compound was synthesized from precursor **5** and compound **9**. Final purification was achieved by column chromatography (SiO_2) using a gradient of CH_2Cl_2/CH_3OH (99:1 v/v) as eluent, affording **15** as a red solid (0.042 g, 70% yield). ^{1}H NMR ($CDCl_3$), δ ppm: 8.16 (s, 1H, H_a); 8.48 (dd, 4H, $H_{4'}$, $H_{7'}$, H_4, and H_7); 8.07 (s, 2H, H_b); 7.78 (s, 2H, $H_{5'}$ and $H_{6'}$); 7.67 (s, 2H, H_5 and H_6); 7.51 (d, 2H, $H_{3'}$ and $H_{8'}$); 7.42 (s, 2H, H_d); 7.32 (d, 2H, H_3 and H_8); 7.07 (d, 4H, $H_{o'}$); 6.74 (d, 4H, H_o); 5.82 (d, 4H, $H_{m'}$); 5.67 (d, 4H, H_m); 4.62 (s, 4H, H_g); 4.80-3.00 (m, oligo(ethylene glycol) linker); 2.44 (s, 3H, CH_3 group). MALDI-TOF: *m/z* found 1447.6229 [M – PF_6]$^+$, calcd 1447.5253 for $C_{81}H_{80}N_{10}O_{12}Cu$.

Electrochemical and Photophysical Studies. All solvents used were purchased from commercial suppliers (spectroscopic grade; 99.5 %) and used without further purification. A single-compartment, three electrode cell configuration was used for the square wave voltammetry measurements, using a glassy carbon electrode (3 mm diameter) as a working electrode, a platinum wire as a counter and a silver wire as a reference electrode. All electrochemical measurements were performed with a METROHM FRA 2 µAutolab Type III potentiostat. For the photophysical characterization the samples were placed in fluorimetric cuvettes with different pathways and, when necessary purged with molecular oxygen or argon. Steady-state UV-vis absorption spectroscopy was performed on a Lambda2 spectrometer (Perkin Elmer). Steady state fluorescence spectra were carried out at a FluoroMax3 spectrometer (Horiba) in the visible detection range and at a FluoroLog3 spectrometer (Horiba) with a IGA Symphony (512x1x1 □m) detector in the NIR detection range (singlet oxygen quantum yields). Fluorescence lifetimes were determined by the time correlated single photon counting technique using a FlouroLog3 emission spectrometer (Horiba JobinYvon) equipped with an R3809U-58 MCP (Hamamatsu) and an N-405LH laser diode (Horiba JobinYvon) exciting at 403 nm (675 ps fwhm). Femtosecond transient absorption (TA) experiments were carried out with an amplified Ti:Sapphire laser system CPA-2110 fs laser (Clark MXR: output 775 nm, 1 kHz, and 150 fs pulse width) using a transient absorption pump/probe detection system (TAPPS Helios, Ultrafast Systems). The 420 nm excitation wavelength was generated with a noncolinear optical parametric amplifier (NOPA, Clark MXR). For the, excitation wavelength the energy of 200 nJ/ pulse was selected. Nanosecond transient absorption experiments were carried out with a Nd:YAG laser. The 532 and 355 nm excitation wavelength was formed by second and third harmonic generation, respectively. Pulse widths of 6 ns with energies of up to 10 mJ were selected. The optical detection was based on a pulsed Xenon lamp, a monochromator, a photomultiplier tube or a fast silicon photodiode with a 1 GHz amplification and a 500 MHz digital oscilloscope. The laser power of every laser pulse was registered using a bypath with a fast silicon photodiode. The experiments were performed on solutions in a 5x10 mm quartz glass cuvette.

Acknowledgements

Notes and references

[a] Department of Chemistry and Pharmacy and Interdisciplinary Center for Molecular Materials, Friedrich-Alexander-Universität Erlangen-Nürnberg, D-91058 Erlangen, Germany.
[b] Department of Chemistry, New York University, New York, NY 10003, USA.
[c] Present address: Institute of Chemistry, University of Campinas, PO Box 6154, Campinas, SP, 13084-861, Brazil.

† Footnotes should appear here.

Electronic Supplementary Information (ESI) available: [details of any supplementary information available should be included here]. See DOI: 10.1039/b000000x/

1 J. Deisenhofer and J. R. Norris, *The Photosynthetic Reaction Center*; Academic Press: New York, 1993.
2 D. M. Guldi, *Chem. Soc. Rev.* 2002, **31**, 22.
3 J. Deisenhofer, O. Epp, I. Sinning and H. Michel, *J. Mol. Biol.* 1995, **246**, 429.
4 J. Deisenhofer and H. Michel, *Science* 1989, **245**, 1463.
5 D. Gust, T. A. Moore and A. L. Moore, *Acc. Chem. Res.* 2001, **34**, 40.
6 D. Gust, T. A. Moore and A. L. Moore, *Acc. Chem. Res.* 2009, **42**, 1890.
7 J. D. Megiatto Jr., A. Antoniuk-Pablant, B. D. Sherman, G. Kodis, M. Gervaldo, T. A. Moore, A. L. Moore and D. Gust, *Proc Natl Acad Sci U S A* 2012, **109**, 15578.
8 P. L. Anelli, P. R. Ashton, R. Ballardini, V. Balzani, M. Delgado, M. T. Gandolfi, T. T. Goodnow, A. E. Kaifer, D. Philp, P. Marek, L. Prodi, M. V. Reddington, A. M. Z. Slawin, N. Spencer, J. F. Stoddart, C. Vicent and D. J. Williams, *J. Am. Chem. Soc.* 1992, **114**, 193.
9 P. R. Ashton, V. Balzani, A. Credi, O. Kocian, D. Pasini, L. Prodi, N. Spencer, J. F. Stoddart, M. S. Tolley, M. Venturi, A. J. P. White and D. J. Williams, *Chem. Eur. J.* 1998, **4**, 590.
10 P- R. Ashton, T. T. Goodnow, A. E. Kaifer, M. V. Reddington, A. M. Z. Slawin, N. Spencer, J. F. Stoddart, C. Vicent and D. J. Williams, *Angew. Chem. Int. Ed. Engl.* 1989, **28**, 1396.

11 D. B. Amabilino, C. O. Dietrich-Buchecker, A. Livoreil, L. Pérez-García, J.-P. Sauvage and J. F. Stoddart, *J. Am. Chem. Soc.* 1996, **118**, 3905.
12 Y.-Z. Hu, D. van Loyen, O. Schwarz, S. Bossmann, H. Dürr, V. Huch and M. Veith, *J. Am. Chem. Soc.* 1998, **120**, 5822.
13 C. O. Dietrich-Buchecker and J.-P. Sauvage, *Tetrahedron Lett.* 1983, **24**, 5095.
14 C. O. Dietrich-Buchecker and J.-P. Sauvage, *J. Am. Chem. Soc.* 1984, **106**, 3043.
15 C. O. Dietrich-Buchecker and J.-P. Sauvage, *Chem. Rev.* 1987, **87**, 795.
16 C. O. Dietrich-Buchecker and J.-P. Sauvage, *Tetrahedron* 1990, **46**, 503.
17 J.-P. Sauvage and C. O. Dietrich-Buchecker, *Molecular Catenanes, Rotaxanes and Knots*; Wiley VCH: Weinheim, Germany, 1999.
18 L. Flamigni, A. M. Talarico, J. C. Chambron, V. Heitz, M. Linke, N. Fujita and J.-P. Sauvage, *Chemistry* 2004, **10**, 2689.
19 L. Flamigni, A. M. Talarico, S. Serroni, F. Puntoriero, M. J. Gunter, M. R. Johnston and T. P. Jeynes, *Chemistry* 2003, **9**, 2649.
20 K. Li, P. J. Bracher, D. M. Guldi, M. A. Herranz, L. Echegoyen and D. I. Schuster, *J. Am. Chem. Soc.* 2004, **126**, 9156.
21 K. Li, D. I. Schuster, D. M. Guldi, M. A. Herranz and L. Echegoyen, *J. Am. Chem. Soc.* 2004, **126**, 3388.
22 J. D. Megiatto Jr., K. Li, D. I. Schuster, A. Palkar, M. A. Herranz, L. Echegoyen, S. Abwandner, G. Miguel and D. M. Guldi, *J. Phys. Chem. B* 2010, *114*, 14408.
23 J. D. Megiatto Jr., D. I. Schuster, S. Abwandner, G. d. Miguel and D. M. Guldi, *J. Am. Chem. Soc.* 2010, **132**, 3847.
24 J. D. Megiatto Jr., D. I. Schuster, G. d. Miguel, S. Wolfrum and D. M. Guldi. *Chem. Mater.* 2012, **24**, 2472.
25 J. D. Megiatto Jr., R. Spencer and D. I. Schuster, *Org. Lett.* 2009, **11,** 4152.
26 D. I. Schuster, K. Li, D. M. Guldi and J. Ramey, *Org. Lett.* 2004, **6**, 1919.
27 L. Flamigni, V. Heitz and J.-P. Sauvage, *Struct. Bond.* 2006, **121**, 217.
28 T. J. Kesti, N. V. Tkachenko, V. Vehmanen, H. Yamada, H. Imahori, S. Fukuzumi and H. Lemmetyinen, *J. Am. Chem. Soc.* 2002, **124**, 8067.
29 T. Umeyama and H. Imahori, *J. Phys. Chem. C* 2013, **117**, 3195.
30 R. A. Marcus, *J. Chem. Phys.* 1956, **24**, 966.
31 D. M. Guldi and S. Fukuzumi, In *Fullerenes: From Synthesis to Optoelectronic Properties*; D. M. Guldi, N. Martin, Eds.; Kluver Academic Publishers: Dordrecht, 2002, p 237.
32 H. Imahori and Y. Sakata, *Adv. Mater.* 1997, **9**, 537.
33 D. M. Guldi, *Chem. Commun.* 2000, 321.
34 D. M. Guldi and M. Prato, M. *Acc. Chem. Res.* 2000, **33**, 695.
35 S. Kirner, M. Sekita and D. M. Guldi, *Adv. Mater.* 2014, **26**, 1482.
36 K. Kadish, E. Van Caemelbecke, G. Royal, In *The Porphyrin Handbook*; K. M. Kadish, M., Smith, R. Guilard, Eds.; Academic Press: New York, 2000.
37 M. E. El-Khouly, Y. Araki, O. Ito, S. Gadde, A. L. McCarty, P. A. Karr, M. E. Zandler and F. D'Souza, *Phys. Chem. Chem. Phys.* 2005, **7**, 3163.
38 F. D'Souza, G. R. Deviprasad, M. E. Zandler, V. T. Hoang, A. Klykov, M. VanStipdonk, A. Perera, M. E. El-Khouly, M. Fujitsuka and O. Ito, *J. Phys. Chem. A* 2002, **106**, 3243.
39 F. D'Souza, M. E. El-Khouly, S. Gadde, A. L. McCarty, P. A. Karr, M. E. Zandler, Y. Araki and O. Ito, *J. Phys. Chem. B* 2005, **109**, 10107.
40 A. S. D. Sandanayaka, N. K. Subbaiyan, R. Chitta, Y. Araki, O. Ito and F. D'Souza, *J. Porphyrins Phthalocyanines* 2008, **12**, 857.
41 J. D. Megiatto Jr. and D. I. Schuster, In *Handbook of Carbon Nano Materials*; F. D'Souza, K. M. Kadish, Eds.; World Scientific Publishers: Singapore, 2011; Vol. 1, p 207.
42 R. Huisgen, *Angew. Chem, Int. Ed.* 1968, **7**, 321.
43 H. C. Kolb, M. G. Finn and K. B. Sharpless, *Angew. Chem. Int. Ed.* 2001, **40**, 2004.
44 C. W. Tornøe, C. Christensen and M. Meldal, *J. Org. Chem.* 2002, **67**, 3057.
45 J. D. Megiatto Jr. and D. I. Schuster, *New J. Chem.* 2010, **34**, 276.
46 J. D. Megiatto Jr., R. Spencer and D. I. Schuster, *J. Mater. Chem.* 2011, **21**, 1544.
47 J. D. Megiatto Jr., D. Patterson, B. D. Sherman, T. A. Moore, D. Gust and A. L. Moore, *Chem Commun (Camb)* 2012, **48**, 4558.
48 L. Echegoyen and L. E. Echegoyen, *Acc. Chem. Res.* 1998, **31**, 593.
49 A. Hirsch and M. Brettreich, *Fullerenes: Chemistry and Reactions*; Wiley-VCH: Weinheim, 2005.
50 F. D'Souza, G. R. Deviprasad, M. E. Zandler, M. E. El-Khouly, M. Fujitsuka and O. Ito, *J. Phys. Chem. B* 2002, **106**, 4952.
51 P. G. Seybold and M. Gouterman, *J. Mol. Spectros.* 1969, **31**, 1.
52 Y.-P. Sun, G. E. Lawson, J. E. Riggs, B. Ma, N. Wang and D. K. Moton, *J. Phys. Chem. A* 1998, **102**, 5520.
53 C. Tanielian and C. J. Wolff, *Phys. Chem.* 1995, **99**, 9825.
54 R. Schmidt and E. Afshari, *J. Phys. Chem.* 1990, **94**, 4377.
55 C. Luo, D. M. Guldi, H. Imahori, K. Tamaki and Y. Sakata, *J. Am. Chem. Soc.* 2000, **122**, 6535.
56 N. Armaroli, M. A. J. Rodgers, P. Ceroni, V. Balzani, C. O. Dietrich-Buchecker, J.-M. Kern, A. Bailal and J.-P. Sauvage, *Chem. Phys. Lett.* 1995, **241**, 555.
57 T. Gunaratne, M. A. J. Rodgers, D. Felder, J.-F-Nierengarten, G. Accorsi and N. Armaroli, *Chem. Commun.* 2003, 3010.

Journal Name ARTICLE

Synthesis and Photophysical Properties of New Catenated Electron Donor-Acceptor Hybrid Systems with Magnesium and Free Base Porphyrins as Donors and C_{60} as the Acceptor

Sabrina V. Kirner,[a] Dirk M. Guldi,[a] Jackson D. Megiatto, Jr.[b, c] and David I. Schuster[b]

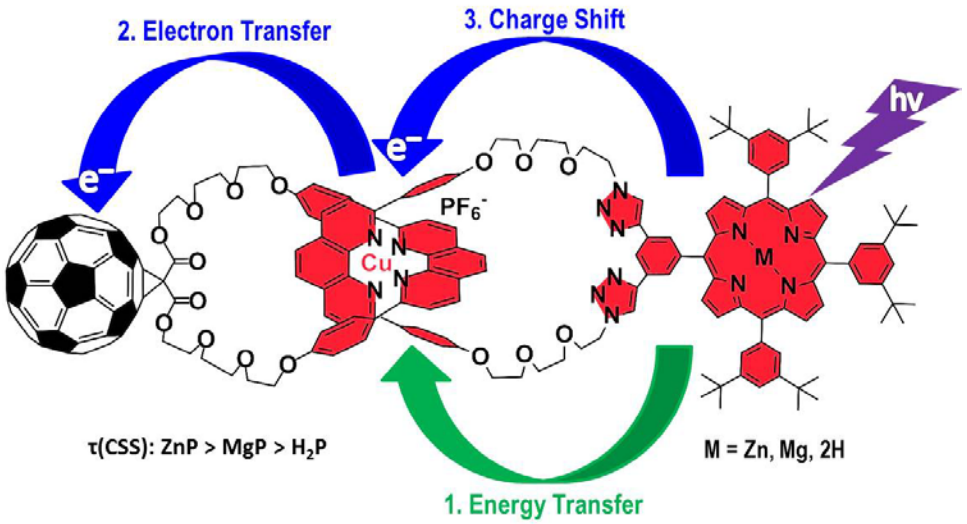

Nanoscale electron donor-acceptor systems with [2]catenane architectures, with magnesium porphyrin (MgP) or free base porphyrin (H_2P) as electron donor and C_{60} as electron acceptor, have been synthesized and the electronic events following photoexcitation have been elucidated.

Journal Name RSCPublishing

ARTICLE